Institute for Geophysics, Astrophysics, and Meteorology
University of Graz

Atmospheric Remote Sensing and Climate System Research Group
ARSCliSys – on the art of understanding the climate system

IGAM/UniGraz Technical Report for ESA/ESTEC No. 2/2004

ESA studies:

ACEPASS – LEO-LEO Occultation Characterisation Study
[ESA/ESTEC Contract No. 16743/02/NL/FF, WP4: LEO-LEO Performance and Sensitivity Analysis]

ACECLIM – ACE+ Climate Impact Study
[ESA/ESTEC Contract No. 17479/03/NL/FF, WP200: Climate Simulation and Analysis]

The Atmosphere and Climate Explorer Mission ACE+: Scientific Algorithms and Performance Overview

G. Kirchengast [1], J. Fritzer [1], M. Schwaerz [1], S. Schweitzer [1], and L. Kornblueh [2]

1) IGAM/University of Graz, Graz, Austria
2) MPI for Meteorology, Hamburg, Germany

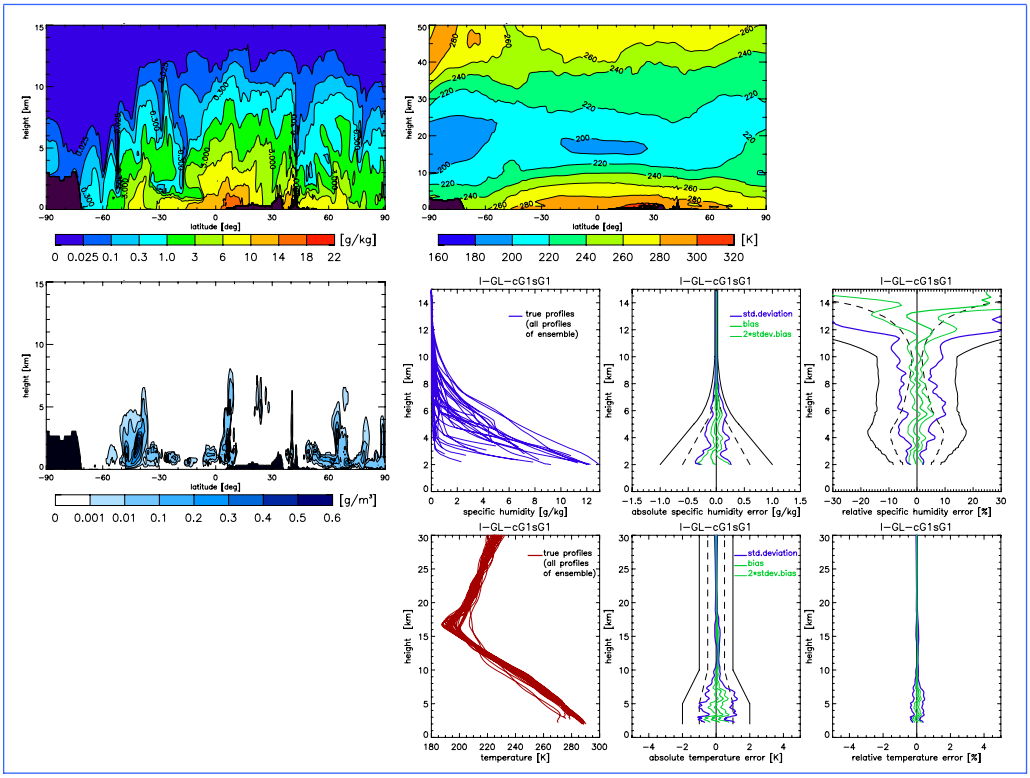

February 2004

(intentionally left blank, back page if double-sided print)

Table of Contents

(intentionally left blank, back page if double-sided print)

1. Introduction

The ACE+ mission, of which an artistic view is provided by Figure 1, is a next-generation radio occultation mission currently prepared by the European Space Agency (ESA). It was proposed by an international scientific team led by Per Hoeg (DMI, Copenhagen, Denmark) and Gottfried Kirchengast (IGAM/University of Graz, Austria) and pre-selected in May 2002 as ESA's top priority future Earth Explorer Opportunity Mission.

The ACE+ constellation of four Low Earth Orbit (LEO) satellites will use Global Navigation Satellite System (GNSS) signals from the GPS and GALILEO systems as well as novel LEO-to-LEO crosslink signals for atmospheric sounding by radio occultation. The measurement principle is that the radio signals, while passing the atmosphere from transmitter to receiver satellite, are refracted and absorbed in a way allowing accurate determination of key variables of atmosphere and climate such as humidity and temperature. ACE+ can provide such data globally, with unprecedented accuracy, high vertical resolution, and long-term stability.

ACE+ aims to quantify climatic variations and trends throughout the free troposphere and stratosphere so as to improve the understanding of processes such as climate feedbacks and external forcing variations. ACE+ will establish highly accurate and vertically resolved climatologies of humidity in the troposphere and of temperature and geopotential height of pressure levels in both troposphere and stratosphere. This will, for example, allow rigorous validation, testing, and improvement of atmospheric models in support of climate research and numerical weather prediction. Important contributions will also be made to other fields such as atmospheric processes research and space weather.

The scientific retrieval algorithms and the demonstration of the capability to meet the demanding performance requirements — which for ACE+ have been laid out by the ACE+ Mission Advisory Group of ESA in a Mission Requirements Document (ACE+ MRD, 2004) — are key elements for assessing the scientific feasibility of the mission and its potential to fulfill its ambitious objectives.

This report provides an overview on the scientific algorithms developed and advanced during Phase A (section 2) as well as an overview on the performance results achieved (section 3). The clear evidence from the scientific performance analyses during Phase A is that ACE+ can fulfill the mission objectives laid out in the ACE+ MRD.

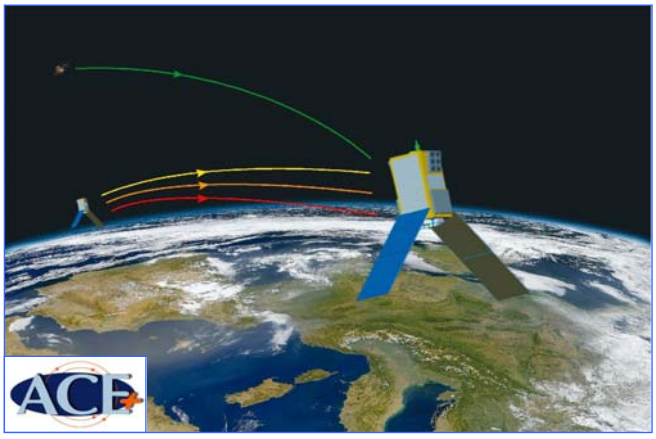

Figure 1: Illustration of the ACE+ concept, indicating both LEO-LEO and GNSS-LEO occultation.

2. Scientific Algorithms Overview

The users of data products obtained from the ACE+ scientific data processing will come from a variety of fields. The primary users will be scientific institutions, mostly from the fields of climate science, meteorology, and atmospheric physics but also, for example, from the ionosphere and space weather community. Furthermore, public services (e.g., weather and climate services, environmental protection services), industrial users, and other international user community interest groups will use ACE+ products.

These different users have varying needs for ACE+ data products, so that the scientific processing has to provide different products from Level 1b basic geo-located products (e.g., bending angle and transmission profiles) via Level 2 geophysical products (e.g., refractivity, humidity, and temperature profiles) to higher-level value-added products (e.g., global 3D humidity and temperature climatologies). Core users, mostly from within scientific institutions and weather and climate services, will, for example, often exploit the Level 1b data products and produce their own higher-level products and use ACE+ data together with other data for purposes like climate change analyses and numerical weather prediction (NWP). Many other users will use Level 2 products or value-added higher-level products (e.g., atmospheric profile products, climate monitoring products, NWP analysis products).

In the scientific algorithms overview below, the focus is placed on describing status and requirements of the Level 1-to-Level 2 processing ("Scientific processing" or "Level 2 processing" hereafter), i.e., on the geophysical profile retrieval algorithms (section 2.1). The "raw processing" down to Level 1 will be addressed in separate ACE+ technical documents. The wide field of processing towards higher-level products is touched on in the context of briefly discussing data assimilation techniques (section 2.2). For more information on the variety of scientific objectives to be served by such products see Kirchengast and Hoeg (2004).

2.1. ACE+ Retrieval Algorithms and Scientific Data Products

Scientific processing implies the application of retrieval techniques to derive geophysical data (Level 2 products) from the Level 1 data. In this process, care has to be taken not only on deriving the profiles themselves but also on precise knowledge of their error characteristics. Also, quality checks need to be performed at all levels.

Figure 2.1 shows a high level sketch of how the ACE+ measurements may be processed by a retrieval system. In particular, for the retrieval of atmospheric parameters, two cases must be considered, GNSS-LEO processing and LEO-LEO processing, respectively.

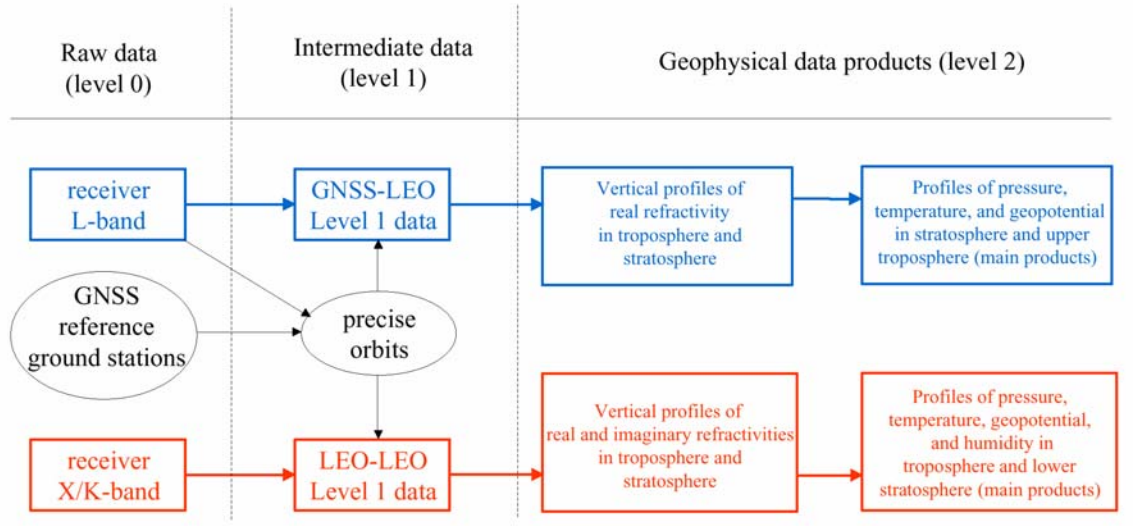

Figure 2.1: Data flow for the generation of ACE+ level 2 data products.

Here the established GNSS-LEO processing is briefly treated first (subsection 2.1.1), followed by the LEO-LEO processing (subsection 2.1.2) and a summary on the Level 1b and Level 2 data products (subsection 2.1.3).

2.1.1. Scientific Processing of GNSS-LEO Occultation Data

The scientific processing of GNSS-LEO data was developed in the framework of other occultation missions such as GPS/MET, CHAMP/GPS, and METOP/GRAS, and is now fairly mature (e.g., Melbourne et al., 1994; Hoeg et al., 1995; Kursinski et al., 1997; Syndergaard, 1999; Steiner et al., 1999; GRAS-SAF, 2000; Healy and Eyre, 2000; Rieder and Kirchengast 2001; Steiner et al., 2001; Hajj et al., 2002).

Figure 2.2 provides a schematic overview on the GNSS-LEO scientific processing. Briefly, the processing starts from Level 1b bending angle profiles available as a function of impact parameter, $\alpha(a)$, and proceeds via (real) refractivity profiles as a function of geometrical height, $N(z)$, to the retrieval of density, pressure (or geopotential height), temperature, and water vapor pressure/humidity profiles ($\rho(z)$, $P(z)$, $T(z)$, $e(z)$, $q(z)$). The bending angle profiles themselves derive from phase delay data, in case of geometric-optics processing, or phase delay and amplitude data, in case of wave-optics processing applied in the lower troposphere (e.g., Jensen et al., 2003).

The key data in the process are accurate Doppler shift data, which directly relate to the bending angle data. The Doppler shift corresponds to the time-derivative of the phase delay, which is the observable that can be very accurately measured over the duration of ~1 min during a GNSS-LEO occultation event.

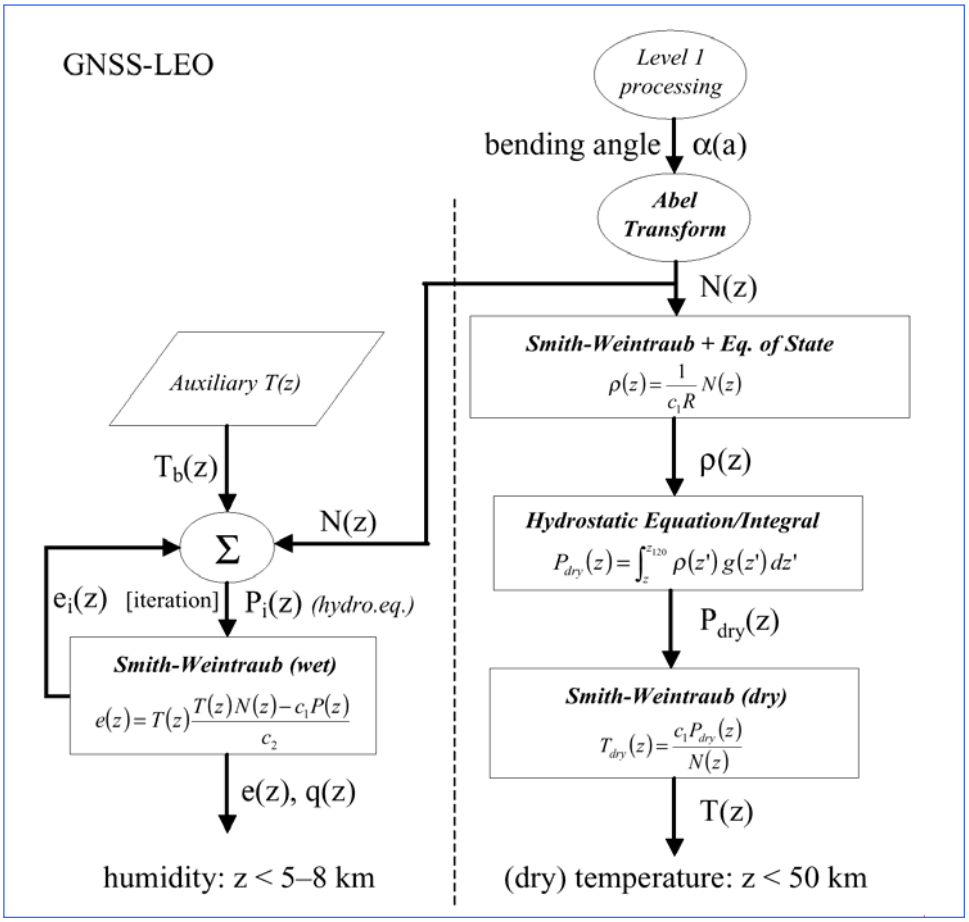

Figure 2.2: Schematic view of the GNSS-LEO level 2 processing.

This accuracy is ensured by the high short-term stability (over ~1–100 sec) of on-board Ultra-Stable Oscillator (USO) frequency standards. Exactly here is the heart of the often quoted intrinsic self-calibration of refractive occultation data: each single Doppler shift profile in itself, together with its associated precise orbital state profiles from Precise Orbit Determination (POD), is an absolute measure of the height-dependent atmospheric bending angle at the time and geographic location of the event, independent of any auxiliary calibration data and of any other measurements before, in parallel, or after the 1-min event. This is also the basis for notions like “unique climate benchmark measurements” or “unique long-term stability over decades from short-term stability over seconds”.

Mathematically, the processing as illustrated in Figure 2.2 is a well-posed essentially linear (except in the lower troposphere) retrieval problem involving simple fundamental equations only such as an Abelian Transform (Fjeldbo et al., 1971), the (real) refractivity equation (Smith and Weintraub, 1953), the hydrostatic equation, and the equation of state. In the troposphere, where water vapor is relevant below about 5–8 km (e.g., Kursinski et al., 1997), separation of temperature and humidity from refractivity requires background (a priori) information, e.g., via a background temperature profile, $T_b(z)$, as indicated for simplicity in Figure 2.2, or via 1D-Var retrieval (Healy and Eyre, 2000). A detailed algorithmic description can be found in Kirchengast et al. (2004) and the references cited above, among which in

particular the reviews by Kursinski et al. (1997), Syndergaard (1999), and Steiner et al. (2001) are instructive.

The main areas where further GNSS-LEO algorithm advancements are being worked on include wave-optics based processing in the lower troposphere (e.g., Gorbunov, 2002; Jensen et al., 2003), improved retrievals in the upper stratosphere (e.g., Gobiet and Kirchengast, 2004), improved error characterization (e.g., Marquardt and Healy, 2003; Steiner and Kirchengast, 2004), and open-loop tracking data processing (e.g., Sokolovskiy, 2001). The processing of open-loop data requires particular attention in future also in Europe. While so far no real instrument data of this type exist, the data from METOP/GRAS, the first instrument with adequate capabilities in terms of SNR and fully-fledged open-loop measurement mode, will certainly spur these activities.

2.1.2. Scientific Processing of LEO-LEO Occultation Data

The scientific processing of LEO-LEO occultation data starts from phase and amplitude data, supplemented by the necessary geometric information, and proceeds via Doppler shifts, bending angles, and transmissions down to quasi-vertical atmospheric profiles of real and imaginary refractivities, density, pressure, geopotential height, temperature, humidity, and liquid water. The algorithms consist of the following main steps:

1. bending angle and transmission retrieval,
2. real and imaginary refractivities retrieval,
3. atmospheric profiles retrieval.

Bending angle and transmission retrieval as well as refractivities retrieval proceed similarly to the GNSS-LEO case and will be only briefly addressed below. The emphasis is placed on the atmospheric profiles retrieval, where a description of a robust optimal estimation processing scheme is given. More details on the algorithms can be found in Kirchengast et al. (2004) and Nielsen et al. (2003), with complementary information also, e.g., in Kursinski et al. (2002) and Kursinski et al. (2004). The processing chain was implemented as part of the End-to-end Generic Occultation Performance Simulator, version 5 (EGOPS5), which was developed in course of the ESA-ACEPASS (ACE+ Phase A Scientific Support) study on LEO-LEO characterisation, based on heritage from the GNSS-LEO simulator EGOPS4 (Kirchengast et al., 2002).

Bending Angle and Transmission Retrieval

The phase and amplitude profiles are used together with the corresponding POD data comprising positions and velocities of LEO transmitter and LEO receiver satellites to determine the atmospheric bending angle profile as a function of impact parameter in the same way as in the well-known GNSS-LEO processing. If wave-optics processing is utilized, both phase path changes (Doppler shift profiles) and normalized amplitude profiles (raw transmission profiles) are used in this process, whereas if geometric-optics processing is performed only Doppler shift profiles are used.

The amplitude profiles at each LEO-LEO signal frequency (ACE+ nominal frequencies near 9.7 GHz, 17.25 GHz, 22.6 GHz), the impact parameter profile, and the transmitter and

receiver position profiles are used to compute the transmission profiles due to atmospheric absorption at each frequency. The exact way to subtract amplitude defocusing and spreading from the measured amplitude profiles, in order to obtain the transmission profiles due to absorption only, depends on whether wave-optics or geometric-optics processing is utilized.

A key step in transmission retrieval is the normalization to a reference height "above the absorptive atmosphere", where the transmission is unity (~25 km in the ACE+ case). This is the step where the intrinsic self-calibration of the amplitudes comes in: similar to the self-calibrated bending angles, this normalization implies that as long as the transmission measurements are short-term stable over the ~30 sec of the occultation event from about 25 km towards the surface, each individual profile is a self-standing reliable measure of the atmospheric absorption at the given place and time, independent of any other measurements. Moreover, since the imaginary refractivity (or absorption coefficient) obtained from the transmission depends on the impact parameter-derivative of transmission only, a small constant transmission residual does not matter.

Real and Imaginary Refractivities Retrieval

The bending angle profile as a function of the impact parameter is converted to the real refractivity profile as a function of height via the classical GNSS-LEO Abel transform. Based on this, the real refractivity profile and the impact parameter profile are used together with the transmission profiles at each LEO-LEO frequency to derive the imaginary refractivity profiles as a function of height with another Abel transform akin to the classical one (same Abelian integration kernel but different in integrand; Kursinski et al., 2002; Kirchengast et al., 2004). Since imaginary refractivity is proportional to the absorption coefficient, the latter can be obtained alternatively or in addition.

If data assimilation of LEO-LEO data products is performed, the refractivity profiles obtained will be the Level 2 data products most conveniently used in such schemes, since both real and imaginary refractivities are, at any point in space and time, just local functions of the atmospheric parameters.

Atmospheric Profiles Retrieval

The real and imaginary refractivity profiles are associated with four equations: three equations from the frequency dependent imaginary refractivity profiles (N^I_1, N^I_2, N^I_3) and one equation from the real part (N^R), because this is practically non-dispersive for the considered frequencies. While the equation for the real part is a simple formula (Smith and Weintraub, 1953), the equations behind the imaginary refractivity as a function of the atmospheric parameters are more elaborated and embodied in a Millimeter-wave Propagation Model (MPM) (e.g., Liebe et al., 1993). Together with the hydrostatic equation and the equation of state, there is a set of six equations to derive the four desired atmospheric parameters: pressure, temperature, humidity and liquid water. The latter, cloud liquid water, is retrieved as a by-product since it can have a strong impact on the absorption signal and is an important parameter for both climate science and meteorology.

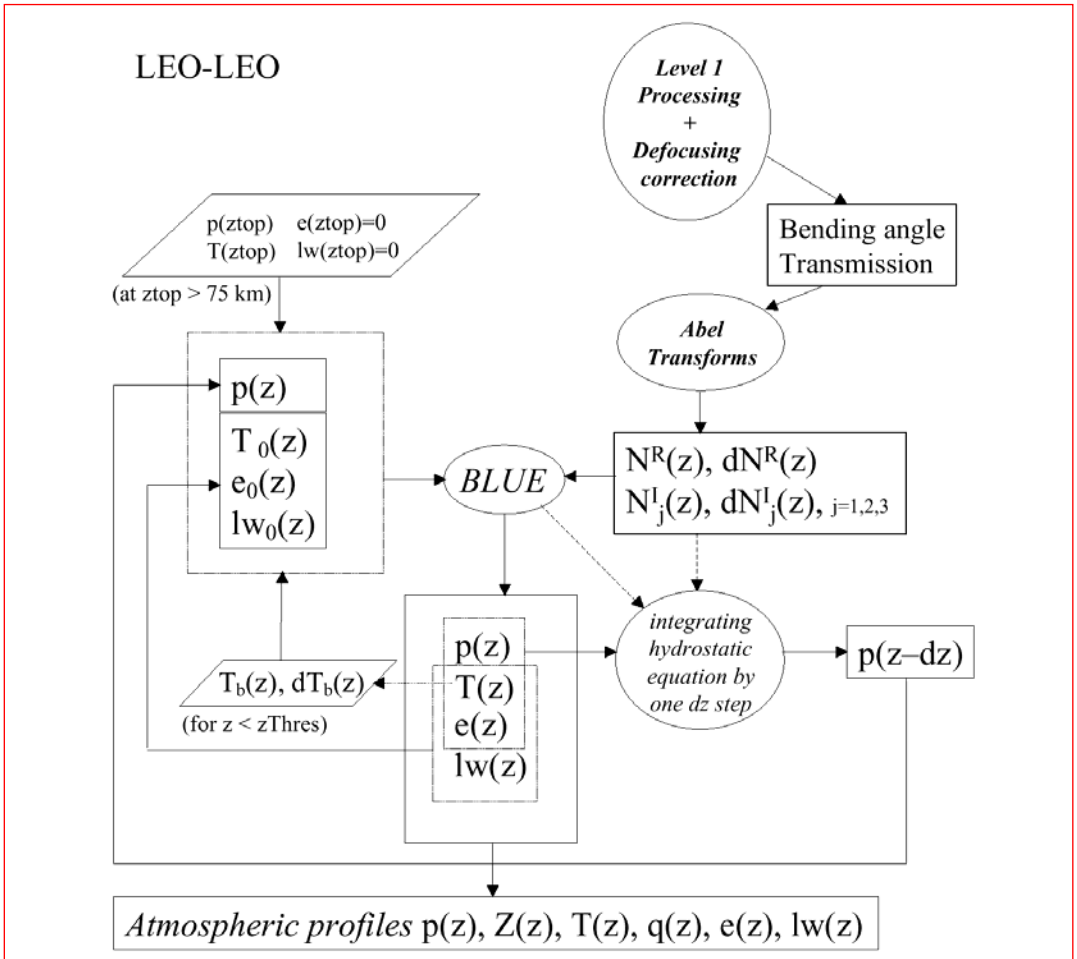

BLUE (Best Linear Unbiased Estimator):

Baseline case ($z_{Thres} = 0$): $\boldsymbol{x}_{n+1} = \boldsymbol{x}_n + \left(\boldsymbol{K}_n^T \cdot \boldsymbol{C}_y^{-1} \cdot \boldsymbol{K}_n\right)^{-1}\left[\boldsymbol{K}_n^T \boldsymbol{C}_y^{-1}\left(\boldsymbol{y} - \boldsymbol{y}_n^{\mathrm{mod}}\left(\boldsymbol{x}_n\right)\right)\right]$

In case of severe turbulence for $z < z_{Thres}$ (z_{Thres} about 3 to 6 km):

$$\boldsymbol{x}_{n+1} = \boldsymbol{x}_n + \left(\boldsymbol{K}_n^T \cdot \boldsymbol{C}_y^{-1} \cdot \boldsymbol{K}_n + \boldsymbol{C}_b^{-1}\right)^{-1}\left[\boldsymbol{K}_n^T \boldsymbol{C}_y^{-1}\left(\boldsymbol{y} - \boldsymbol{y}_n^{\mathrm{mod}}\left(\boldsymbol{x}_n\right)\right) - \boldsymbol{C}_b^{-1}\left(\boldsymbol{x}_n - \boldsymbol{x}^b\right)\right]$$

$\boldsymbol{x}_n$: state vector to be (iteratively) estimated
$\boldsymbol{y}_n$, $\boldsymbol{y}_n^{\mathrm{mod}}$: measurement vector, forward-modeled measurement vector
$\boldsymbol{C}_y$: measurement (and forward modeling) error covariance matrix
$\boldsymbol{K}_n$: Jacobian weighting matrix
$\boldsymbol{x}^b$: background (a priori) state vector
$\boldsymbol{C}_b$: background (a priori) error covariance matrix

Figure 2.3: Schematic view of the LEO-LEO level 2 processing.

Figure 2.3 schematically illustrates the LEO-LEO Level 2 processing with particular emphasis on the atmospheric profiles retrieval. The retrieval begins at a topmost layer and works downward towards the surface at height steps of 100 m or smaller. The problem of retrieving the atmospheric state (pressure *p*, temperature *T*, water vapor pressure *e*, cloud liquid water density *lw*) from the refractivities (N^R, N^I_1, N^I_2, N^I_3) is efficiently solved by a downward integration of the hydrostatic equation, to sequentially obtain *p*, combined with an iterative Best Linear Unbiased Estimation (BLUE) solution (Rodgers, 2000) at each

integration step to obtain (T, e, lw) from (p, N^R, N^I_1, N^I_2, N^I_3). The BLUE algorithm is initialized by the atmospheric state obtained at the previous height level. The hydrostatic integration provides the pressure "backbone" for this estimation and ensures it to be very robust and reliable. The BLUE requires the specification of covariance matrices for the refractivity data, which are formulated based on the knowledge of their respective error characteristics. The initialization of the whole algorithm is made at high altitudes (e.g., 75 km) with some initial state (p_{top}, T_{top}, e_{top}=0, lw_{top}=0), the accuracy of which is non-critical as initialization errors decay quickly over about the first two to three scale heights.

Practically, above a certain height above which water vapor has a negligible effect (~20 km), only T is estimated. Furthermore, above a certain height above which liquid water is negligible (~8 km), only (T, e) is estimated. Below, the full state (T, e, lw) is estimated, which requires at least 3 independent elements of information in (p, N^R, N^I_1, N^I_2, N^I_3). Due to the insensitivity to ice clouds (e.g., Gradinarsky et al., 2003), no ice water retrieval is needed.

Because the set of equations is somewhat over-determined, it is still possible to retrieve all desired parameters if one of the imaginary refractivity information pieces is lost, as it will be the case at any given height level, where only two of the three frequencies provide amplitude data in useful dynamic range. The information on real refractivity at the lowest of the transmitted frequencies will be lost only in extreme (and rare) situations. If the imaginary refractivity variances grow large enough into the lower troposphere so as to render the BLUE problem effectively underdetermined, which can happen in case of atmospheric turbulence, the advanced processing described below will be used.

Processing in case of severe atmospheric turbulence

Strong amplitude scintillations due to atmospheric turbulence can introduce significant noise into the imaginary refractivity data and may degrade the above baseline retrieval of atmospheric profiles below about 3 to 6 km in the troposphere. However, since the parts of the signal affected by scintillation can be identified thanks to the high sampling rate of the raw measurements (1 kHz), this enables a constant monitoring of the high frequency fluctuations and the determination of a "threshold height", z_{Thres}, below which the imaginary refractivity data should be used with caution and potentially receive low to negligible weight in the BLUE process. As turbulence is a layered phenomenon (e.g., Gage, 1990), usually only some fraction of the height levels below z_{Thres} may need to receive such down-weighting. This will have to be confirmed in future studies. In the performance analyses of section 3 it has been assumed, as a conservative limit, that the complete height range below any z_{Thres} found is filled with turbulence and is down-weighted.

In case of down-weighting applied to imaginary refractivities below z_{Thres}, one sensible way to cure the consequent under-determination of the BLUE problem is to introduce weak background (a priori) information into the retrieval at the height levels concerned. The primary candidate information for this purpose is temperature, since it is well predictable in the troposphere above the boundary layer and since it is sufficient auxiliary information under all conditions to ensure a robust estimation. Suitable background temperature profiles (T_b) can be obtained from a profile search in an adequate database (e.g., from a 24h ECMWF forecast in a geographic area of some degrees around the profile co-located with the measurement). The T_b profile selected can be the one that best fits the retrieved temperature profile in the troposphere right above z_{Thres}, where the retrieved data are still very accurate and allow for a

good fit. The fit to the retrieved data, and not just selection of a co-located profile, is to avoid importing any potential small bias from the background into the retrieval (though ECMWF temperatures below 8 km are essentially unbiased). In producing the performance results for section 3 below, this "best-fit *T* extrapolation" approach has been used for heights below z_{Thres} and found to ensure accurate humidity and temperature retrieval also under severe turbulence conditions.

The algorithm described above already provides satisfactory results (see section 3), although it is not yet particularly optimized. In the future, algorithms for severe turbulence situations will have to be studied in more detail in order to ensure optimal solutions. Other techniques, such as wave-optics approaches (e.g., Full Spectrum Inversion; Jensen et al., 2003), can perhaps be used to reduce scintillation fluctuations already on the transmission measurements (Level 1b) so that less down-weighting of imaginary refractivity data will be required at the atmospheric profiles retrieval step.

As the LEO-LEO component is the novel part of ACE+, future processing advancements are possible and required at all steps of the retrieval chain: From detailed performance analyses of different methods to derive transmission profiles (both geometric-optics and wave-optics based) to optimized atmospheric profiles retrieval (both without and with presence of turbulence), future developments shall ensure exploitation of the LEO-LEO data in the best possible manner.

2.1.3. Level 1b and Level 2 Data Products

The scientific processing discussed above provides conversion of basic geo-located Level 1 data (phase delays/Doppler shifts and amplitudes/raw transmissions) via bending angles (GNSS-LEO) or bending angles and transmissions (LEO-LEO) to Level 2 atmospheric profiles. In order to obtain a clear overview on the ACE+ data products available in this process at Level 1b and Level 2, Table 2.1 below gives a summary on the main products.

The product domain will be global, and from 2 km to 50 km in height for most products; humidity products will be available throughout the troposphere, covering 2 km to 15 km. All Level 1b and Level 2 products will be available to users within 30 days of observation time, and a significant fraction of the data also in near-real time for NWP, i.e., within 3 hrs of observation time (on a best-effort basis).

Detailed performance requirements on the scientific data products are found in the Mission Requirements Document (MRD) of the ACE+ Mission Advisory Group of ESA (ACE+ MAG, 2004). The ACE+ MRD also provides a more detailed list of data products from Level 0 to Level 2.

Table 2.1: Main ACE+ Level 1b and Level 2 data products.

Level	GNSS-LEO	LEO-LEO
Level 1b	• Doppler shift and Raw Transmission [(1)] profiles (at L1+L2) vs. time • Bending angle profiles vs. impact parameter	• Doppler shift and Raw Transmission [(1)] profiles (at 3 frequencies) vs. time • Bending angle profiles vs. impact parameter • Transmission profiles (at 3 frequencies) vs. impact parameter
Level 2	• Real Refractivity profiles vs. height • Humidity profiles vs. height • Temperature profiles vs. height • Pressure and Geopotential Height profiles vs. height • Error estimates and meta-data for all retrieved level 1b & level 2 profiles	• Real Refractivity profiles vs. height • Imaginary Refractivity profiles (at 3 frequencies) vs. height

[(1)] "Raw Transmission" is the normalized received power ($P(t)/P_{above\text{-}atmos}$) including defocusing and absorption, whilst the "Transmission" includes absorption only (*Transmission* = 1 – *Absorption*).

2.2 ACE+ Processing by Data Assimilation Techniques

The ACE+ measurements shall be extensively exploited via data assimilation schemes, both alone as climate benchmark data for purposes such as climate model validation, testing, and improvement as well as together with other upper air and surface observations for re-analysis purposes. The importance and various modes of employing data assimilation to ACE+ data have been described by ESA (2001), Hoeg and Kirchengast (2002), and Kirchengast and Hoeg (2004). Only a brief account is given here.

Because of the high accuracy of the retrieved climate data, the basic direct diagnosis of climate variations during the mission period is relatively straightforward using modern assimilation techniques. A more difficult problem is, as one example, to isolate those variations that are due to external forcing from those internal to the climate system, mainly because the mission period is short compared to the typical time scales of internal climate variability. However, by assimilating the observed occultation data into the atmospheric component of a climate model it is possible to monitor variations in the model's fit to the observations (e.g., Hoeg and Kirchengast, 2002).

As one example, Figure 2.4 shows a result of a study by Andersen et al. (2001), where data assimilation was used for detecting volcanic forcing and potential long-term trends based on the ECMWF re-analysis data set "ERA15". The two major volcanic eruptions, El Chichon 1982 and Pinatubo 1991, are clearly seen via anomalous heating rates of up to > 0.25 K/day. In addition, there seems to exist some long-term cooling trend, the reliability of which is questionable, however, due to inhomogeneities in the underlying data. Bengtsson et al. (2004) have found similar problems when aiming at detection of climate trends in using the newer ECMWF re-analysis data set "ERA40". ACE+ data with their accuracy and their long-term stability due to intrinsic self-calibration will be highly valuable to improve this situation. Furthermore, besides for climate uses, assimilation will clearly be the standard way to exploit the data for NWP.

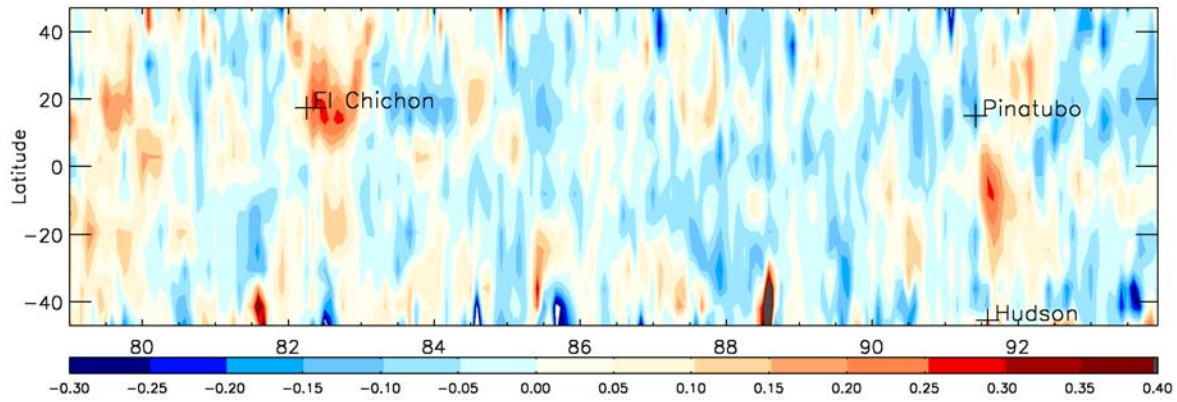

Figure 2.4: Anomalies relative to the average annual cycle in the zonal mean of 24-hr temperature analysis increments (units K/day; 30 hPa level, period 1979–1993, use of ECMWF re-analysis data set "ERA15"). From Andersen et al. (2001).

Basically, the ACE+ observations can be assimilated at four different levels:

1. assimilation of retrieved atmospheric parameters (e.g., humidity, temperature),
2. assimilation of real and imaginary refractivities,
3. assimilation of bending angle and transmission profiles,
4. assimilation of Doppler shifts and raw transmission profiles.

The closer the data are to the atmospheric parameters used by the model, the simpler is the assimilation scheme. On the other hand, the more data processing is carried out on the measured signals, the more difficult it is to accurately specify the required observation error covariance matrices. For example, the error covariances of the Doppler shifts and raw transmissions are directly linked to the specifications of the instrument, whereas the error covariances for the retrieved atmospheric parameters must be found through detailed analysis of the error propagation through the processing chain. As a result, pre-retrieval of humidity and temperature profiles, which are then assimilated into models, will not be very sensible.

Assimilation of real and imaginary refractivities, or of bending angle and transmissions, can be statistically optimal using variational techniques, now common in assimilating passive radiance data from satellites. The assimilation of real refractivity has been prepared already (e.g., Healy and Eyre, 2000) and the assimilation of imaginary refractivities would only require the use of a different local refractivity formulation, which is available (a Millimeter-wave Propagation Model instead of the Smith-Weintraub formulation; cf. subsection 2.1.2).

Assimilation of more raw products would require more complex observation operator formulations but would not involve spherical symmetry assumptions. For example, operators can be constructed, which account for horizontal variations through the iterative use of a ray-tracer (e.g., Zou et al., 1999). However, also more simple operators are available for refractivities, which properly account for horizontal variations and spherical asymmetries by modeling "Abelian weighted" refractivity profiles (Syndergaard et al., 2004).

Future advances required in assimilation processing related to ACE+ will include in particular the development and optimization of techniques dedicated to the assimilation of imaginary refractivities and transmissions, as well as the detailed analysis and quantification of error covariance matrices for all retrieved Level 1b and Level 2 data products. In addition, beyond Level 2 processing, advances in climate data assimilation systems for the purposes of model validation, testing, and improvement will be required.

3. Scientific Performance Overview

The ACE+ Mission Advisory Group has laid down in its Mission Requirements Document (MRD) scientific performance requirements ("ACE+ observational requirements") for both LEO-LEO and GNSS-LEO occultation (ACE+ MRD, 2004). The key atmospheric parameters, on which the observational requirements have been defined there, are humidity and temperature. If these requirements are fulfilled it is intrinsically ensured that also the other Level 2 as well as the pre-requisite Level 1b data products are of adequate quality to meet the ACE+ scientific objectives. The performance estimation results below thus focus on humidity and temperature performance.

The ACE+ MRD (2004) also summarized the main system requirements, consistent with the detailed system and instrument requirements provided by ESA to the ACE+ industrial Phase A study consortia. These system and instrument requirements were used as input to the performance analysis, in particular the baselined orbital geometries and the measurement performance specifications at Level 1 data level. The simulations reported on below have been performed consistent with these specifications.

As LEO-LEO occultation is the new technique in ACE+, enabling accurate independent retrieval of humidity and temperature as described in section 2, broadest attention in this overview is given to LEO-LEO performance. The feasibility of the LEO-LEO observations and the compliance of the data product quality with the scientific requirements has been demonstrated and is presented in section 3.1. The performance of the GNSS-LEO occultation has extensively been proven in the past, including with current satellite missions such as CHAMP. The GNSS-LEO performance is thus only briefly re-captured in section 3.2. Finally, the performance of the mission, LEO-LEO and GNSS-LEO together, for quantifying climate variability and trends over the mission lifetime of 5 years is addressed in section 3.3.

3.1. LEO-LEO Occultation Performance

The LEO-LEO performance analysis results discussed below, drawn from comprehensive performance and sensitivity analyses within the ESA-ACEPASS study, demonstrate the compliance with the scientific requirements, in most cases compliance with the target requirements, given in the ACE+ MRD. An end-to-end simulator, including the LEO-LEO retrieval algorithms discussed in section 2, was used for the performance assessment. The simulator, EGOPS5 (End-to-end Generic Occultation Performance Simulator, Version 5), was developed as an advancement and extension of the established EGOPS4 simulator for GNSS-LEO occultation (Kirchengast et al., 2002).

Representative performance assessment scenarios based on both a climatological atmosphere and a ECMWF high-resolution analysis field are discussed. The instrumental errors for all scenarios (thermal noise, instrumental 1/f noise, amplitude drift errors) have been modeled according to the defined system/instrument requirements. The LEO transmitter and receiver orbits have been assumed consistent with the Phase A baseline (orbital heights near 650 km and 800 km, etc.). The vertical resolution of the retrieved profiles is ~1 km for all scenarios shown, in line with the respective target requirements (ACE+ MRD, 2004).

3.1.1. Assessment Based on Climatological Atmosphere Cases

A large number of atmospheric scenarios was analyzed based on the CIRA86aQ moist-air climatology model (Kirchengast et al. 1999), supplemented by a simple cloud model (Eriksson et al., ESA-ACEPASS Team, pers. communications, 2003), and an atmospheric turbulence/scintillation model (Kuhn, 2003; M. Sterenborg et al., ESA/ESTEC, pers. communications, 2003). Five representative CIRA86aQ cases were defined for this purpose, which together cover humidity and temperature conditions from tropical summer to high-latitude winter. The respective humidity and temperature profiles are illustrated in Figure 3.1. The climatological scenarios discussed here all use the mid-latitude summer case, results including the other cases are shown by Kirchengast et al. (2004) and Gradinarsky et al. (2003).

Five scenarios for different representative combinations of cloudiness and atmospheric turbulence have been defined to illustrate the performance under diverse conditions, which are summarized in Table 3.1. These cover conditions from clear-air, non-turbulent to cloudy and severely turbulent. For each scenario, an ensemble of 40 profile realizations was simulated in order to enable statistical performance estimates in terms of standard deviations and biases. The size of the ensembles was limited by the significant computational resources needed for the forward modeling of the simulated data, in particular for the high-accuracy ray-tracing and along-ray absorption integrations involved.

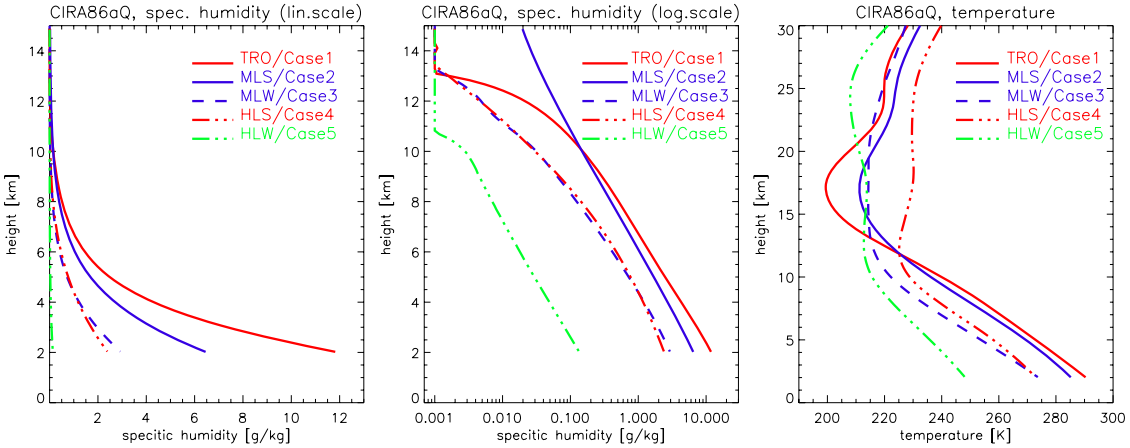

Figure 3.1: Humidity and temperature profiles of five representative atmospheric cases of the CIRA86aQ model: tropical (TRO; July 0°N), mid-latitude summer (MLS; July 40°N), mid-latitude winter (MLW, January 40°N), high-latitude summer (HLS, July 70°N), and high-latitude winter (HLW; January 70°N).

Table 3.1: Parameters for cloud and turbulence scenarios.

1	**clear-air, no turbulence**	(reference scenario)
2	**3D Cirrus clouds ("cCi1") plus "high-latitude" turbulence ("sHL1")** C_{n0}^2 = 1x 10^{-16} $m^{-2/3}$, H_{Cn2} = 2 km	*iwc* = 0.05 g/m^3 ± 0.025 g/m3 (rms; 0–01 g/m^3) *c_height* = 8 km ± 0.5 km (rms; 7–9 km) *c_thickness* = 1.6 km ± 0.4 km (rms; 0.8–2.2 km)
3	**3D Altostratus clouds ("cAs1") plus "mid-latitude" turbulence ("sML1")** C_{n0}^2 = 1.3x 10^{-15} $m^{-2/3}$, H_{Cn2} = 2 km	*lwc* = 0.2 g/m^3 ± 0.1 g/m^3 (rms; 0–0.4 g/m^3) *c_height* = 4.5 km ± 0.25 km (rms; 4–5 km) *c_thickness* = 0.6 km ± 0.15 km (rms; 0.3–0.9 km)
4	**3D Cumulus clouds ("cCu1") plus "subtropical" turbulence ("sST1")** C_{n0}^2 = 1 x 10^{-14} $m^{-2/3}$, H_{Cn2} = 1.5 km	*lwc* = 0.5 g/m3 ± 0.25 g/m^3 (rms; 0–1 g/m^3) *c_height* = 2.5 km ± 0.25 km (rms; 2–3 km) *c_thickness* = 0.3 km ± 0.05 km (rms; 0.2–0.4 km)
5	**3D Cumulonimbus clouds and precipitation ("cCp1") plus "tropical" turbulence ("sTR1")** C_{n0}^2 = 2 x 10^{-13} $m^{-2/3}$, H_{Cn2} = 1 km	*lwc* = 2.5 g/m3 ± 0.5 g/m^3 (rms; 1.5–3.5 g/m^3) *c_height/lwc* = 2 km ± 0.25 km (rms; 1.5–2.5 km) *c_thickness/lwc* = 2 km ± 0.25 km (rms; 1.5–2.5 km) *iwc* = 0.15 g/m3 ± 0.05 g/m^3 (rms; 0.05–0.25 g/m^3) *c_height/iwc* = 9 km ± 0.5 km (rms; 8–10 km) *c_thickness/iwc* = 3 km ± 0.5 km (rms; 2–4 km) *rr* = 20 mm/h ± 5 mm/h (rms; 10–30 km) *rr_topheight* = 2.5 km ± 0.25 km (rms; 2–3 km)

Legend: C_{n0}^2 … turbulence structure constant at surface, H_{Cn2} … scale height of turbulence structure constant, *lwc* … liquid water content (density) of cloud, *c_height* … center height of cloud, *c_thickness* … thickness of cloud about center height, *iwc* … ice water content (density) of cloud, *rr* … rain rate, *rr_topheight* … top height of rainfall. The horizontal extend of clouds was set to 200 km for *Ci* and *As*, 100 km for *Cu*, and 10 km for *Cp*. *Cp* has a gradual *lwc* decay over several kms above *c_thickness/lwc*. The horizontal extend of turbulence was set to 200 km in all cases and the vertical C_n^2 decay was assumed exponential with the scale height H_{Cn2}. The outer scale of turbulence was set to 100 m.

As a reference, the retrieval performance for the clear-air, non-turbulent scenario is shown first in Figure 3.2. The performance is found within target requirements at essentially all heights for both humidity and temperature. Figure 3.2 indicates the unique potential of the technique for determining un-biased humidity and temperature and its particular strength in the upper troposphere as already emphasized by Hoeg and Kirchengast (2002). No threshold height z_{Thres} (on the meaning of z_{Thres} see section 2, subsection 2.1.2 on LEO-LEO retrieval) was reached in the atmospheric profiles retrieval for this turbulence-free scenario, so no down-weighting of imaginary refractivities and best-fit temperature extrapolation from above z_{Thres} is involved.

Figure 3.3 shows empirical results of Sterenborg and Baptista (ESA/ESTEC, pers. communications, 2004) on the turbulence structure constant (C_n^2) of the atmosphere derived from high-resolution radiosonde data at different latitudes. The results are consistent with respective literature evidence on C_n^2 from turbulent scatter radars and in-situ refractometers (e.g., Gage, 1990; Gossard, 1990). This type of results has been used as guideline to define reasonable average (median) turbulence cases for the present performance analysis, as summarized in Table 3.1.

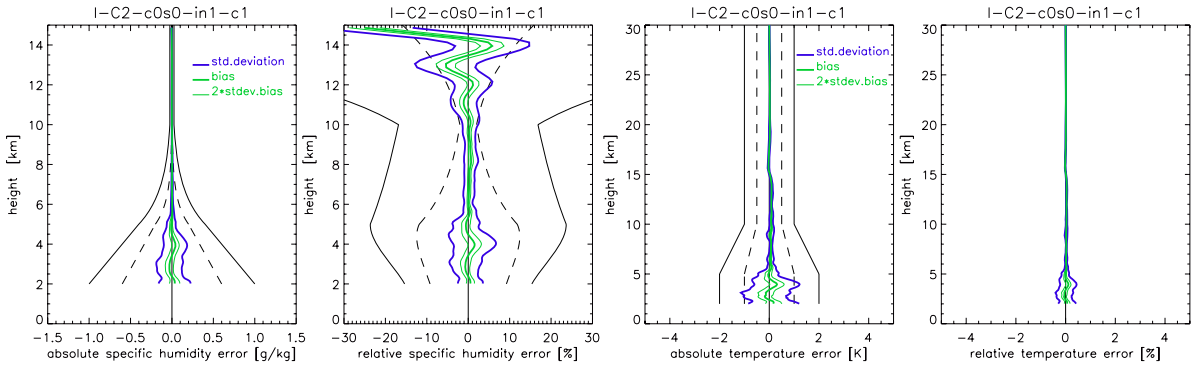

Figure 3.2: Humidity (left panels) and temperature (right panels) retrieval error results for the clear-air, non-turbulent scenario. Statistical performance results are shown (standard deviation, bias, 2 x std.deviation of bias), with the std. deviations depicted as +/– envelopes about the bias profiles. In the left and two middle panels the observational requirements, as laid out in the ACE+ MRD, are shown for reference (solid black, threshold requirements; dashed black, target requirements). The small temperature residual bias of up to 0.1 K visible below 15 km in this and the following Figures 3.4 and 3.7–3.9 is a small technical weakness only of the present not fully optimized end-to-end simulation as is a significant fraction of the "error oscillation" above about 12 km in the relative humidity error.

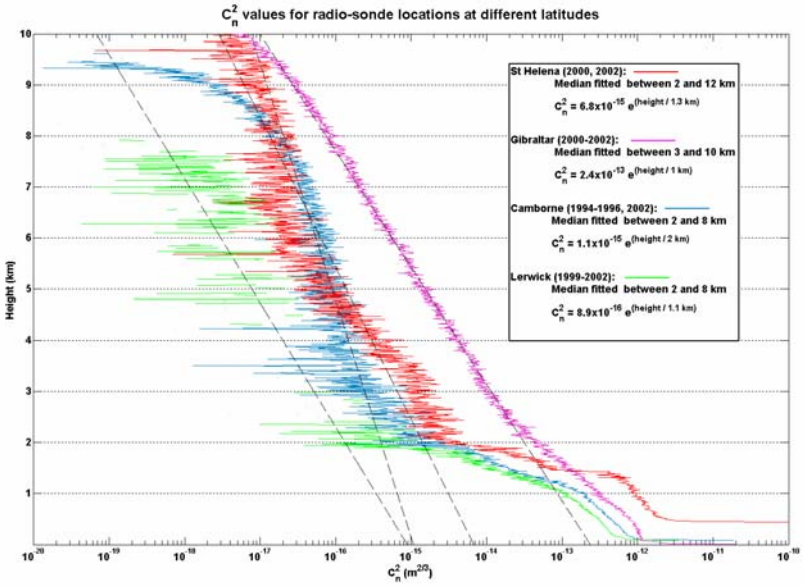

Figure 3.3: Exemplary empirical median C_n^2 profiles, and associated best log-linear fits, derived from multi-year high-resolution radiosonde databases at different latitudes. (Courtesy of M. Sterenborg, ESA/ESTEC, Noordwijk, Netherlands)

The clouds as defined by Table 3.1, with the parameters largely following Gradinarsky et al. (2003) who compiled from literature typical properties of the different cloud types, were essentially modeled as simple horizontally-limited layers with constant liquid water or ice water content within the given thickness about the given cloud height. The clouds where assumed centered at the occultation event (mean tangent point) location ensuring they were passed in their entire extend by the occultation signals. Randomized selection of the cloud parameters within the given bounds was performed to obtain different clouds for the

individual realizations in an ensemble, mimicking cloud variability. Every 2nd event in each ensemble was assumed cloudy, mimicking an average cloud coverage of 50 %.

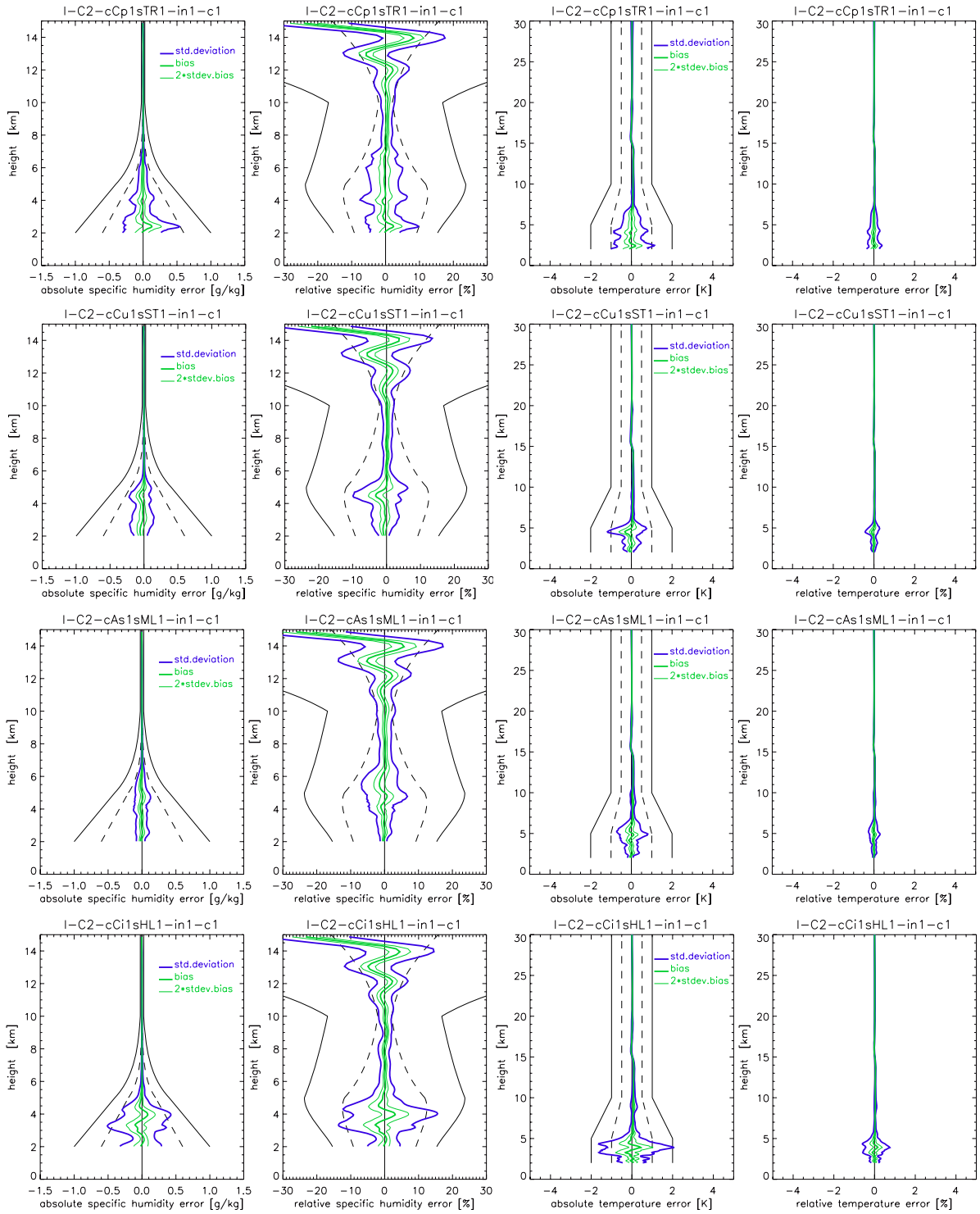

Figure 3.4: Humidity (left panels) and temperature (right panels) retrieval error results for the four cloudy, turbulent air scenarios of Table 3.1. Each row depicts one scenario (top, "tropical"; 2nd, "subtropical"; 3rd, "mid latitude"; bottom, "high latitude"). Figure layout same as Figure 3.2, see that caption for details.

Figure 3.4 shows the humidity and temperature performance results for the four representative cloudy and turbulent scenarios of Table 3.1. All scenarios are found within target requirements and un-biased at almost all heights, and as in Figure 3.2 the upper troposphere between about 6 and 12 km is found particularly accurate with specific humidity errors in general smaller than 5 %. In the lower troposphere, the "high-latitude" (HL) scenario, influenced by the weakest turbulence, exhibits the comparatively largest errors. This is due to the fact that turbulence is now present but that for the given turbulence strength still no threshold height z_{Thres} is reached in most of the realizations of the ensemble, so that almost no auxiliary temperature information is utilized. In the other scenarios, z_{Thres} is reached between about 3 to 6 km, dependent on turbulence conditions.

Below z_{Thres} then auxiliary temperature is involved, leading to accurate retrievals in the lower troposphere also in presence of turbulence. Since here, for simplicity and reference, the best-fit profile search was done in the CIRA86aQ climatology itself (which also contains the "true" mid-latitude summer profile), the results below 5 km can be judged optimistic. However, as the results from the ECMWF cases below show, also a realistic search library with temperature uncertainties of up to 1–2 K is sufficient for retrievals well within requirements in the lower troposphere. The different liquid water clouds are found not to pose significant problems for the retrieval. The presumed insensitivity to ice clouds is found confirmed (see also Gradinarsky et al., 2003), which is important for several ACE+ science objectives (Kirchengast and Hoeg, 2004). Significant rain is found to strongly impact the absorption and to lead to z_{Thres} being found above the top of rain, so that rain has an effect analogous to severe turbulence. Significant rain rates above 2–3 km height are rare, however.

3.1.2. Assessment Based on ECMWF Operational Analysis Cases

As a quasi-realistic performance analysis case an operational T511L60 analysis (~40 km x 40 km horizontal resolution, 60 vertical levels from surface to 0.1 hPa) of the ECMWF was used (12 UTC analysis of Sept. 15, 2002; near-equinox date, otherwise arbitrarily chosen). A global set of about 115 occultation events was simulated (the number limited by the computationally expensive forward modeling as in the previous subsection), drawing every 2$^{\mathrm{nd}}$ event from a day of LEO-LEO measurements, and sorting the events into three latitude bands (low, mid, high). Figure 3.5 illustrates the coverage by ACE+ LEO-LEO occultation events for a baseline 4-satellite constellation (~230 profiles/day) and shows the global distribution of the selected events falling into both cloudy and clear-air areas.

ECMWF analyses contain besides humidity and temperature also 3D liquid water and ice water cloud fields, which were included in the modeling. Figure 3.6 illustrates, via a latitude-height cross-section at 0 deg longitude (Greenwich meridian), the variability of the humidity, temperature, liquid water, and ice water fields in the analysis used. The vertical humidity and temperature profiles at each event location have been used, disregarding the horizontal variation about this location. This was done to clearly quantify the observational and retrieval errors and to avoid mixing in representativeness errors. The latter are small given properly defined "true" profiles (e.g., Foelsche and Kirchengast, 2004; Syndergaard et al., 2004). The present LEO-LEO end-to-end simulator could not yet supply adequate Abelian-weighted "true" profiles, however, but only vertical profiles. The 3D liquid water and ice water fields

have been used as they are and contribute to the absorptive occultation signal at any location where occultation rays pass through cloudiness.

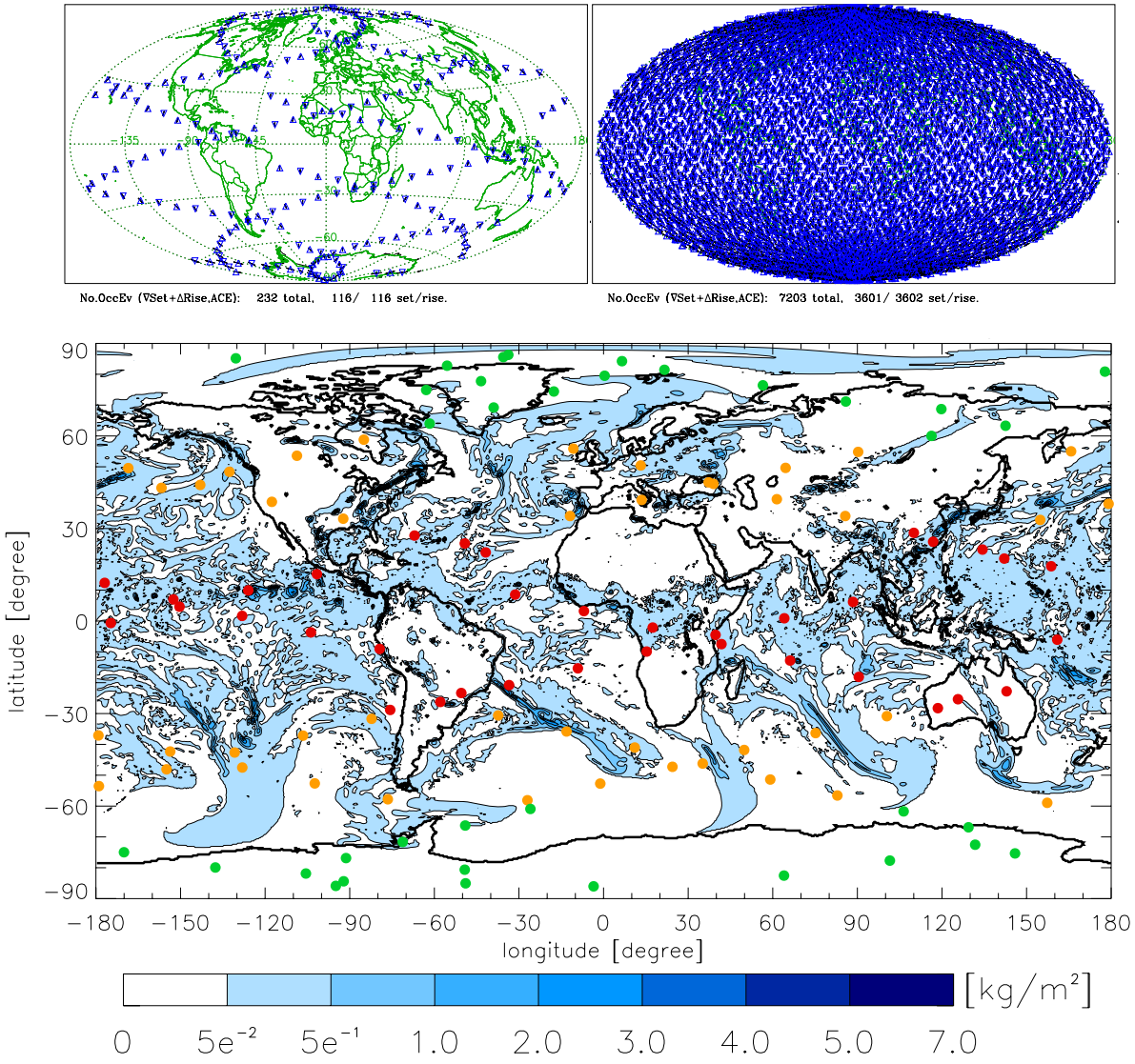

Figure 3.5: Coverage by LEO-LEO occultation events for baseline 4-satellite constellation. Top-left: daily coverage; Top-right: monthly coverage; Bottom: Coverage used in the simulations, including every 2nd daily event sorted into low (red dots), middle (orange dots), and high (green dots) latitude bands of 30 deg width each. The background shows the vertically integrated liquid water density (units g/m^2), indicating cloud coverage (data from Sept. 15, 2002, 12 UTC, ECMWF analysis).

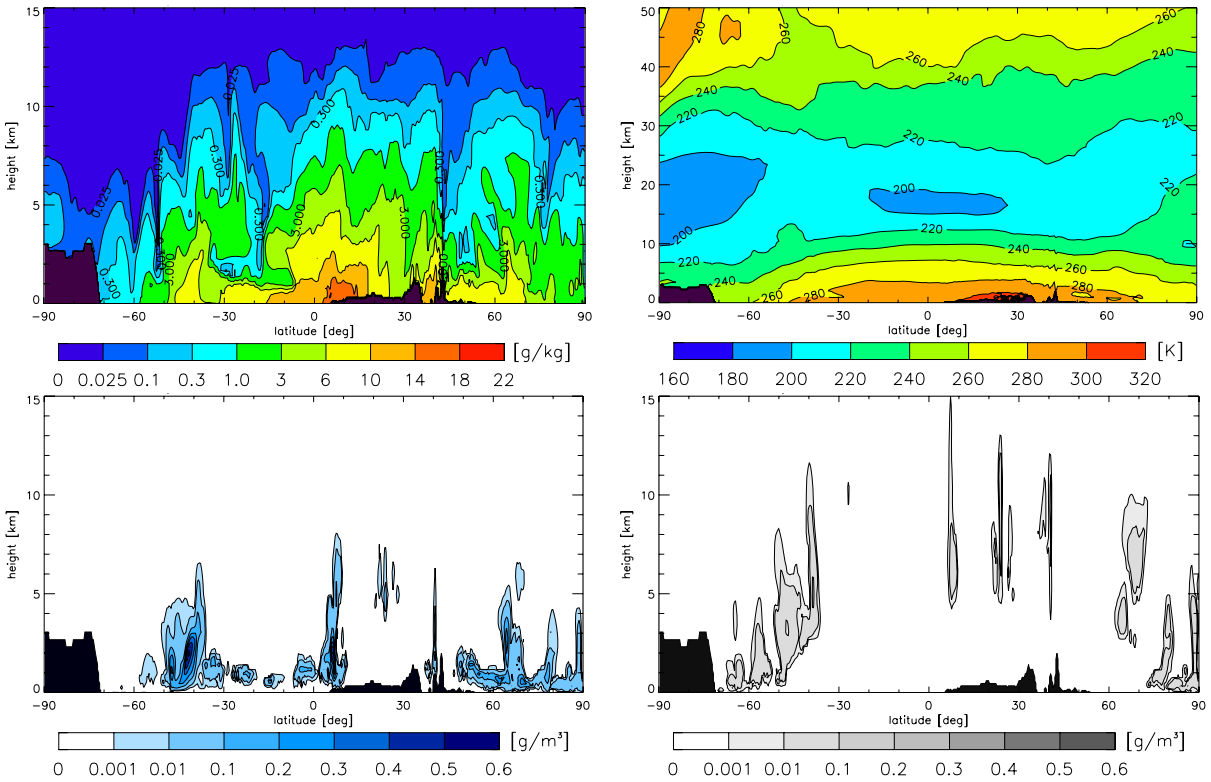

Figure 3.6: Specific humidity (top-left), temperature (top-right), liquid water density (bottom-left), and ice water density (bottom-right) latitude-height cross sections at 0 deg longitude through the ECMWF analysis used in the simulations (analysis of Sept. 15, 2002, 12 UTC).

Regarding turbulence/scintillations, the same model as with the CIRA86aQ cases was used (Kuhn, 2003; M. Sterenborg et al., ESA/ESTEC, pers. communications, 2003) but with the main turbulence parameters modeled as a function of latitude based on the turbulence cases defined in Table 3.1. The values of C_{n0}^2 and H_{Cn2} were assigned to latitudes (both North and South) of 0 deg ("sTR1"), 20 deg ("sST1"), 50 deg ("sML1"), and 70 deg (s"HL1"), complemented by the values ($C_{n0}^2 = 3\text{x}10^{-15}$ m$^{-2/3}$, $H_{Cn2} = 1.75$ km) at 30 deg to better reflect subtropical dry and weakly turbulent areas (ACE+ MAG, pers. communications, 2004). In between, linear interpolation was performed, and beyond 70 deg values were kept constant at the 70 deg values. If due to turbulence best-fit background temperatures needed to be invoked below z_{Thres} (see subsection 2.1.2 for details), temperature profiles from the ECMWF 24h forecast for the analysis time were used as "search library", searching within a few degrees around the given event location. A conservative uncertainty of 0.75 K (near z_{Thres}) to 2 K (near 2 km) was then attached to the best-fit profile.

Figures 3.7 to 3.9 show the performance results for the three latitude bands, each containing an ensemble of about 30–40 occultation events (see Figure 3.5). Not all profiles reach fully down to 2 km, partly due to topography, partly due to multipath effects in the lower troposphere limiting the ray-tracing. Future more elaborated (and computationally expensive) wave-optics forward modeling will cope with the latter effects. From GNSS-LEO experience, the performance found here using ray-tracing forward modeling will not change much, however; tentatively it will be improved.

The left panels of Figures 3.7 to 3.9 illustrate the wide variety of atmospheric humidity and temperature conditions covered by the profiles. The humidity error panels show that the performance is in general found within target requirements below about 6 to 10 km, above it is not far from these well within threshold requirements. No significant biases are found at any height and the humidity errors up to near 10 to 12 km, dependent on latitude, are found within about 10%. Above 10 to 12 km, a considerable fraction of the errors can be attributed to the not yet fully optimized LEO-LEO end-to-end simulator, in particular to improvement potential in the filtering and weighting of transmission and imaginary refractivity data and to the humidity cut-off (to zero) at 15 km by the current atmospheric models inherited from the GNSS-LEO end-to-end simulator (holds for both the CIRA86aQ model and for the current "GCM 3D Atmosphere" model accessing and interpolating the ECMWF analyses). The temperature performance is found unbiased and within target requirements essentially at all heights for all three latitude bands.

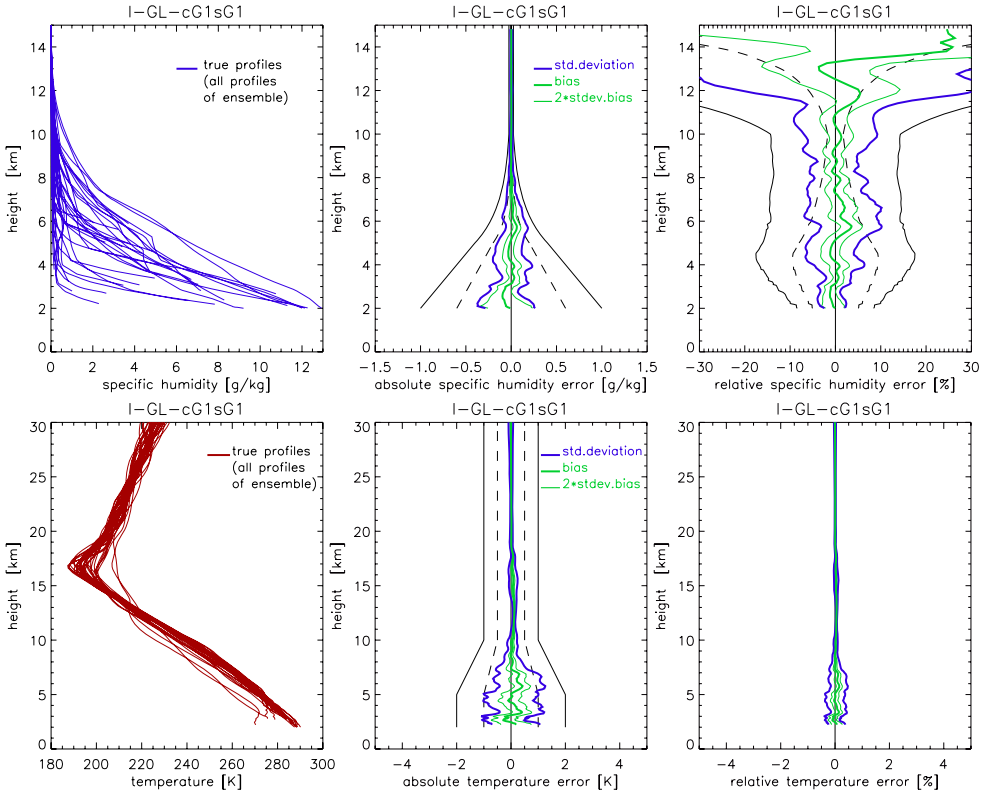

Figure 3.7: Humidity (top) and temperature (bottom) "true" profiles (left panels) and retrieval error results (middle and right panels) for the ECMWF low-latitude ensemble. Error result panels layout as for Figure 3.2, see that caption for details.

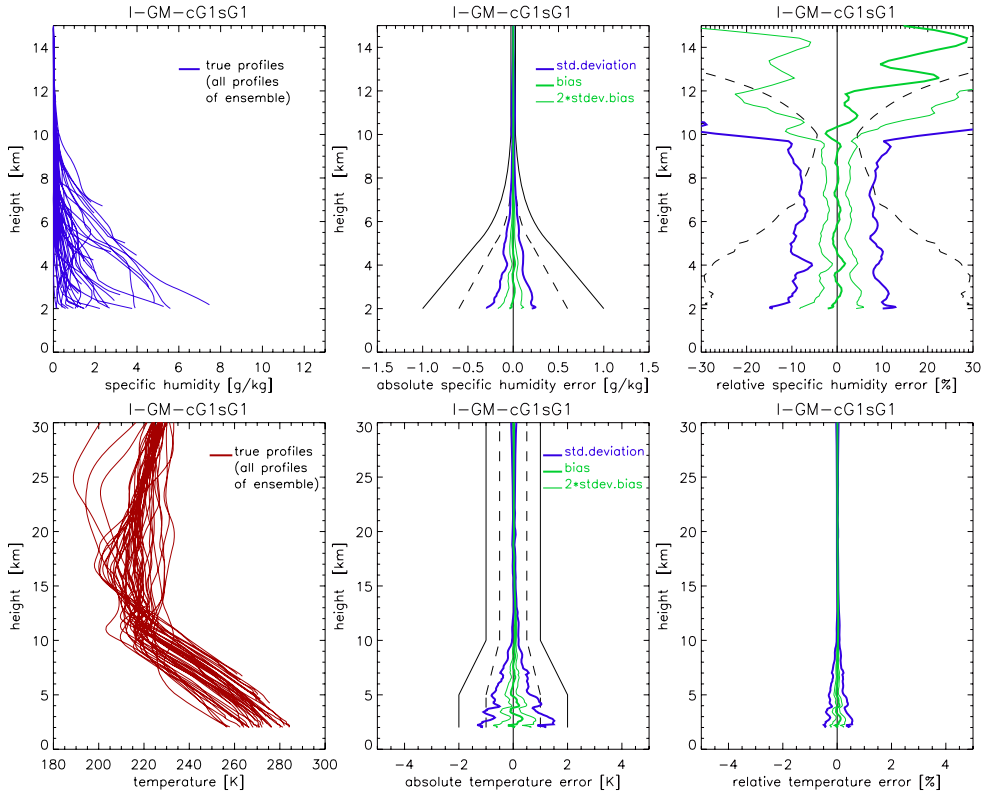

Figure 3.8: Humidity (top) and temperature (bottom) "true" profiles (left panels) and retrieval error results (middle and right panels) for the ECMWF mid-latitude ensemble. Same layout as Figure 3.7.

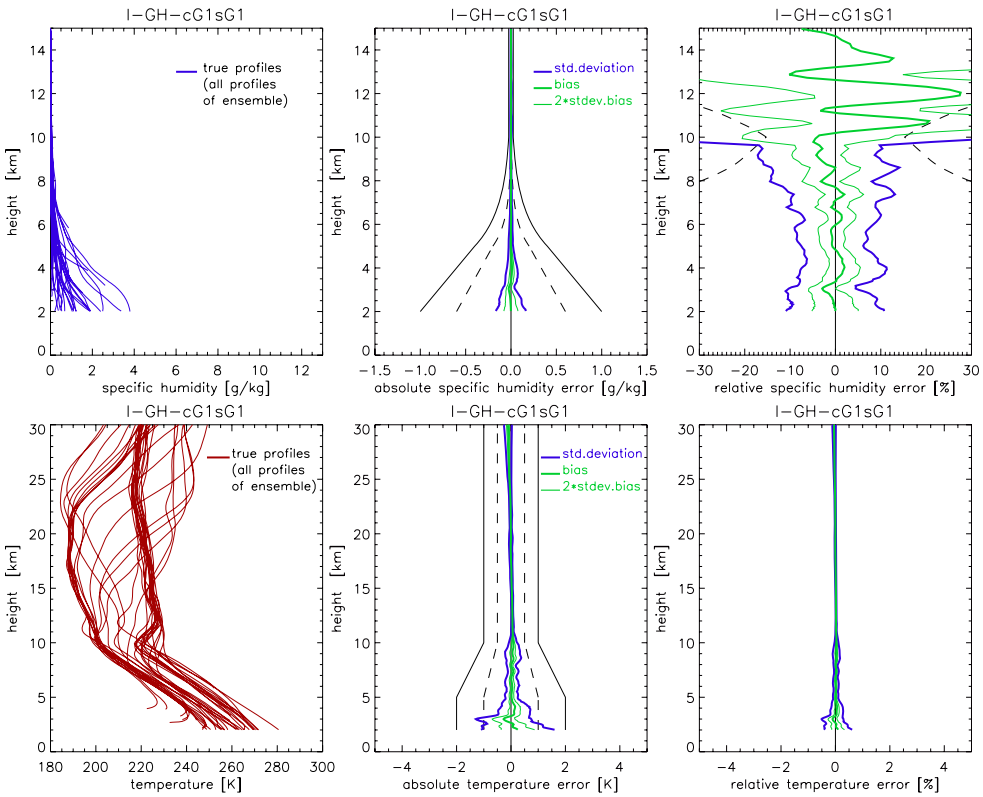

Figure 3.9: Humidity (top) and temperature (bottom) "true" profiles (left panels) and retrieval error results (middle and right panels) for the ECMWF high-latitude ensemble. Same layout as Figure 3.7.

Figure 3.10 illustrates, via retrieval error-to-background error ratios as an instructive diagnostic (e.g., Rodgers, 2000; Rieder and Kirchengast, 2001), the independence of the baseline retrieval (z_{Thres} = 0; see subsection 2.1.2 for details) from background information as well as how background temperature information comes in below about 3 to 6 km dependent on the severity of atmospheric turbulence. Error ratios well below 0.1 imply that essentially all information comes from the measurements, whilst ratios > 0.5 indicate that the majority of information comes from the background.

The error ratio profiles of the clear-air, no-turbulence reference scenario (shown in Figure 3.2) demonstrate that background plays no role in the baseline retrieval. The error ratios of the ECMWF ensembles for the three latitude bands, with strongest turbulence modeled at low latitudes and weakest at high latitudes, indicate how different z_{Thres} of individual events lead in average to temperature background information becoming important (ratios > 0.5) below about 3 km (high latitudes) to 6 km (low latitudes). This is consistent with expectations related to the severity of turbulence (cf. subsection 2.1.2), whereby it is to be re-called that here the most conservative case of fully height-filling turbulence below z_{Thres} was modeled.

Water vapor error ratios are always about zero, independent of whether temperature background is used or not, since water vapor background is never used. At the heights, where temperature background is used, the humidity retrieval is mainly based on the real refractivity measurements plus the background temperature. Figures 3.7 to 3.9 show that the humidity and temperature retrievals are un-biased also at these heights, which is ensured by the best-fit to the retrieved temperature data above z_{Thres} and the quality of the "search library" (24h forecasts here).

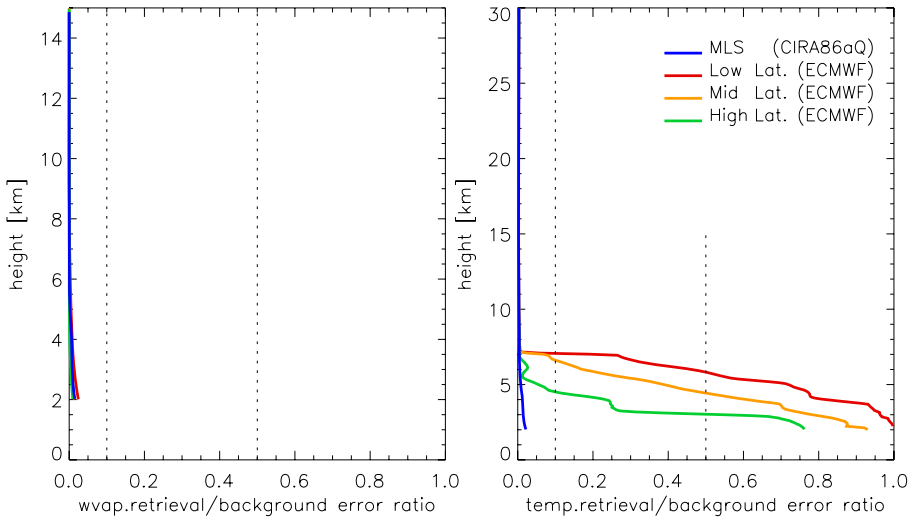

Figure 3.10: Retrieval error-to-background error ratios for retrieved water vapor (left panel) and temperature (right panel) profiles for the clear-air, non-turbulent reference scenario of Figure 3.2 (blue), and the ECMWF low-latitude (red), mid-latitude (orange), and high-latitude (green) ensembles. Baseline background uncertainties in the BLUE algorithm have been set to 100 K and 25 mbar for temperature and water vapor, respectively, for the presented results, but could have been set to any other "quasi-infinite" values, which ensure the BLUE being entirely driven by the measured refractivities only.

In summary, the LEO-LEO performance is found fully compliant with the requirements laid out in ACE+ MRD (2004). Compared to GNSS-LEO with its tropospheric temperature-humidity ambiguity, the simultaneous availability of accurate humidity, temperature, and pressure as function of geometric height from LEO-LEO is a particularly intriguing property. Also the best-fit temperature extrapolation from above z_{Thres} in case of severe turbulence in the lower troposphere, a simple method found adequate for retrieval under these adverse conditions, is enabled by this favorable property.

3.2. GNSS-LEO Occultation Performance

The performance of GNSS-LEO occultations is well established due to the strong heritage of the observation principle and dedicated studies for previous missions. Starting with the successful GPS/MET "proof-of-concept" within 1995–1997 (e.g., Rocken et al., 1997), the GNSS-LEO technique was extensively evaluated and detailed descriptions of the method and its scientific performance are available from literature (e.g., Kursinski et al., 1997; GRAS-SAF, 2000; Lee et al., 2001; Steiner et al., 2001; Hajj et al., 2002; Steiner and Kirchengast, 2004; and references therein). These sources confirm the compliance of GNSS-LEO retrievals with the requirements in ACE+ MRD (2004). Thus for brevity only one illustrative climate-related performance result is included here.

For climate change analyses based on GNSS-LEO data, refractivity, dry temperature, and geopotential height are particularly promising variables. As an example, Figure 3.11 illustrates the dry temperature accuracy (left panel) and indicates that climate trends expected over the coming decades (right panel) will be reliably measurable by GNSS-LEO data thanks to their accuracy and long-term stability.

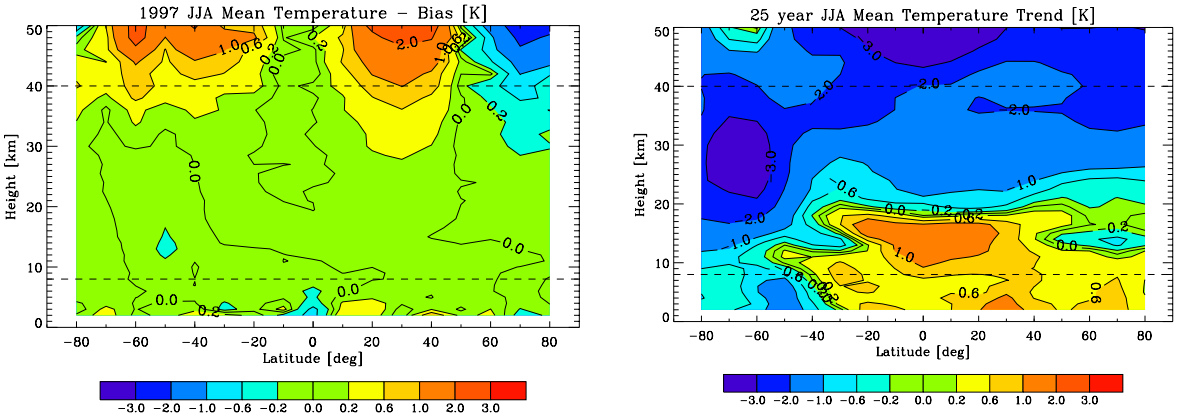

Figure 3.11: Latitude-height slice of climatological residual bias errors in average profiles of dry temperature in 17 latitude bins of 10° width from 80°S to 80°N (left panel) compared to 25-yr summer temperature trends from 2001–2025 in the same bins (right panel). Each average profile in the left panel involves ~50 realistically simulated individual GNSS-LEO occultation profiles sampled by an ACE+-type satellite constellation within a full summer season (June-July-August). The trends in the right panel are derived from a recent climate model simulation with the Hamburg ECHAM5 model at T42L39 resolution (top at 0.01 hPa).

Within the ACE+ concept, the GNSS-LEO data are an important complement to the LEO-LEO data in that they vastly enhance the number of occultation profiles per day and thus importantly contribute to the scientific objectives as is made evident also in the following section.

3.3. Climate Variability and Trends Measurement Performance

Assessing the performance of measuring climate variability and trends over the mission lifetime has been done in form of a check on how adequate the ACE+ coverage is, together with the accuracy demonstrated in the subsections above, in order to reach a required climatological accuracy. As basis for the check, two 5 year climate simulations were run based on observed "AMIP2" sea surface temperature and sea ice information for a control time-slice with present-day climate and based on the IPCC greenhouse gas "SRESa2" scenario (IPCC, 2001) and boundary conditions from the ECHAM4/OPYC GSDIO experiment (Roeckner et al., 1999) for a 2nd time-slice. To be consistent with ACE+ resolution capabilities, the climate model needs good vertical and horizontal resolution. The Hamburg ECHAM5.2/MA model was used in a T106L90 mode, which provided satisfactory resolution, horizontally ~85 km at the equator and ~50 km at mid-latitudes, and 90 levels up to 0.01 Pa (~80 km height). Details on these simulations and the related analyses within the ESA-ACECLIM study can be found in Kornblueh et al. (2004).

Based on the 5 years of model run output fields, humidity and temperature profiles were sampled at all ACE+ LEO-LEO and GNSS-LEO occultation event locations occurring over a 5-yr mission lifetime. The along-ray horizontal resolution of about 300 km was accounted for in this sampling in that not just local but "along-ray weighted" profiles where extracted at each event location. The ACE+ mission used was the baseline 4-satellite constellation (cf. ACE+ MRD, 2004), fall-back to 3 satellites and 2 satellites was used for comparison. The extensive sets of event locations were computed from 5-yr ACE+ geometry simulations with the EGOPS end-to-end simulator propagating the satellites with a long-term accurate Keplerian orbit propagator. Before constructing climatologies, the sampled humidity and temperature profiles where superposed with random errors statistically consistent with the expected LEO-LEO and GNSS-LEO accuracy. ACE+-observed climatologies were then constructed based on the sampled profiles and compared to the "true" climatologies computed from the climate model output at full resolution.

Here global-mean performance results are shown at the 300 hPa level (~9 km) and the 500 hPa level (~5 km), respectively. The required climatological accuracy to reasonable capture climate variability and trends at these levels has been defined, from experience, as 0.1 K for temperature and 5 % for specific humidity at 300 hPa, and as 0.2 K and 5 % at 500 hPa.

Figure 3.12 shows, for the three different ACE+ constellations assumed, the global-mean humidity and temperature errors in the ACE+-observed climatologies relative to the "true" climatologies as a function of the averaging time window up to a seasonal average (90 days). The error level for a time window of one month is a good indicator for sufficient spatial coverage with respect to measuring variability and trends. The smaller the error within 30 days is, the better for climate applications. It is desired that the defined climatological accuracies are reached within 30 days.

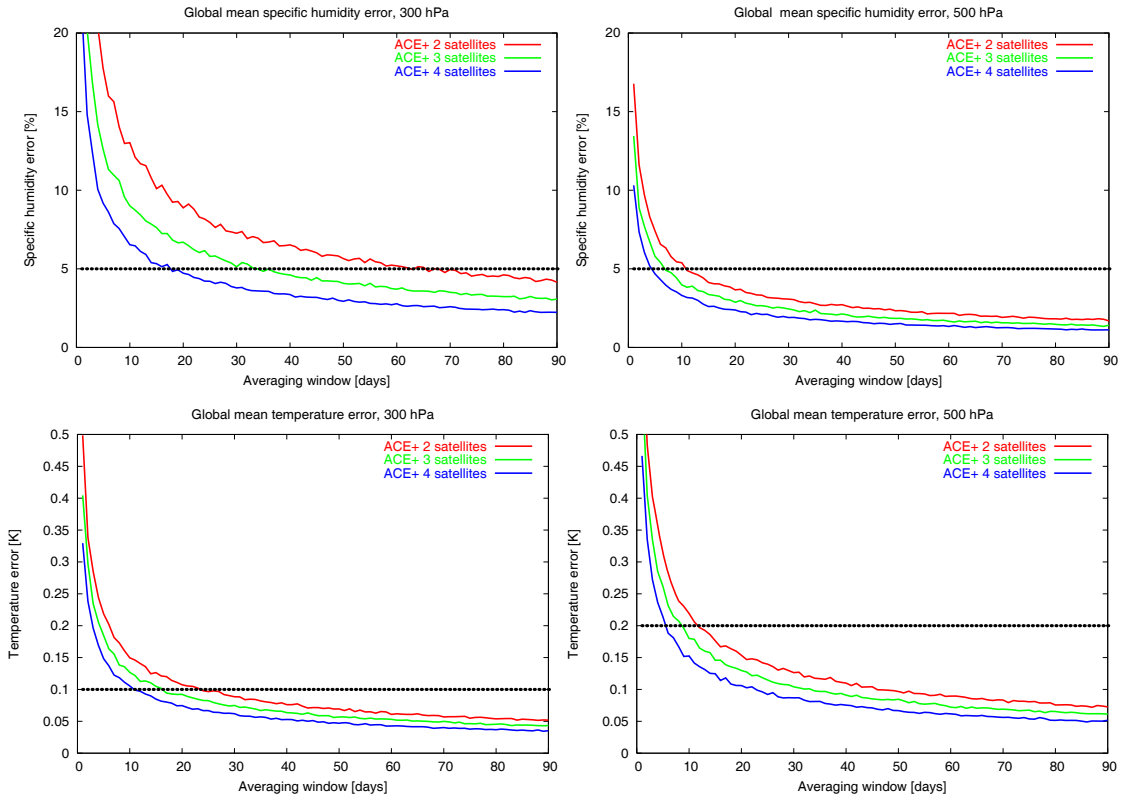

Figure 3.12: Global-mean climatological specific humidity (top) and temperature (bottom) errors at 300 hPa (left) and 500 hPa (right) as function of averaging interval. Results for four (blue), three (green), and two (red) ACE+ satellites are shown and a climatological accuracy desired within < 30 days is indicated (dotted horizontal).

For humidity, the achieved accuracy at the 300 hPa level is dominated by the LEO-LEO data (since GNSS-LEO sensitivity to humidity above 8 km is generally negligible), whilst at 500 hPa the GNSS-LEO data dominate due to their large number (> 4000 GPS/GALILEO occultations per day, ~230 LEO-LEO occultations per day). The upper tropospheric humidity is of particular interest, however. It is found that a 4-satellite constellation is mandatory to achieve the 5% climatological humidity accuracy within one month; the 2-satellite constellation requires more than 2 months sampling to achieve it. For temperature, to which both GNSS-LEO and LEO-LEO contribute important information, the required accuracies are achieved well within one month. This indicates significant climate information potential also at regional scales.

Figure 3.13 shows, for the climate run based on the IPCC scenario, the global-mean, monthly-mean evolution of humidity and temperature at 300 hPa and 500 hPa, with the defined climatological accuracies shown as error bars. Figure 3.13 illustrates that an ACE+ 4-satellite constellation, in reaching the accuracy levels within 30 days, is able on the level of monthly means to capture the original global climate evolution, including in upper tropospheric humidity. By reducing the number of satellites this ability is degrading, which practically means that longer-term and larger-area averaging has to be done to reach a certain climatic accuracy and that the respective information on smaller-scale climate variability is lost.

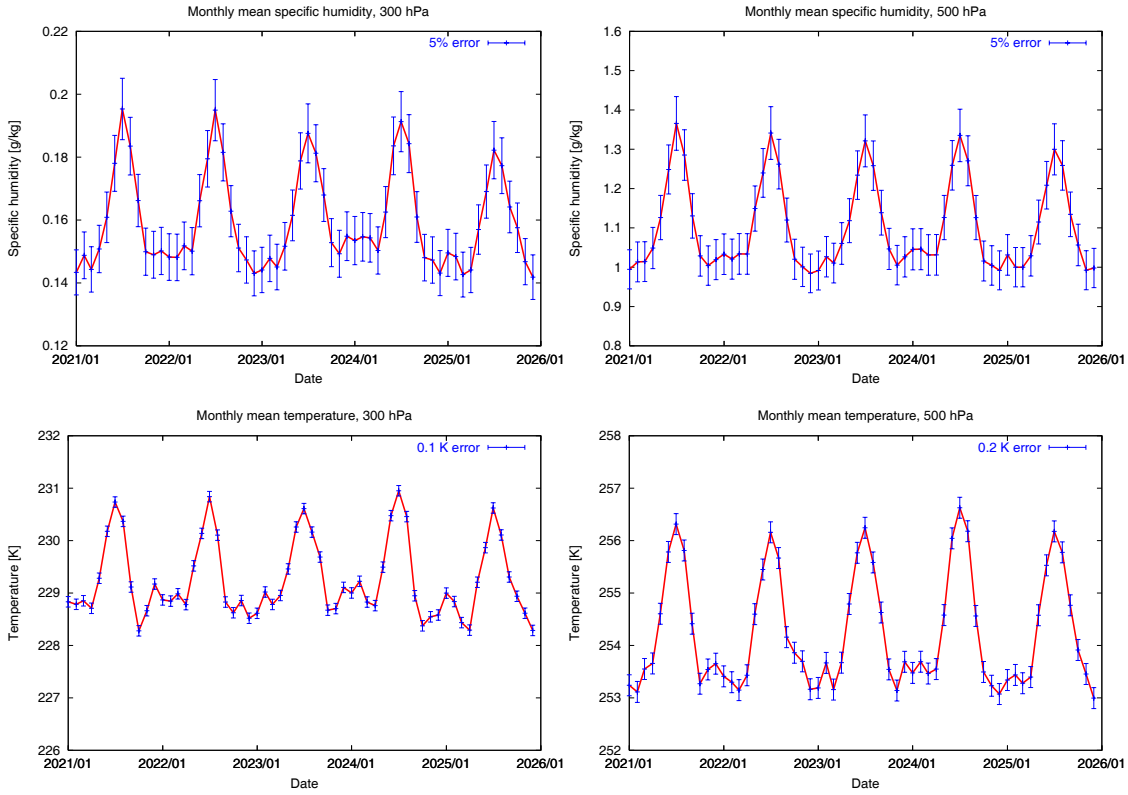

Figure 3.13: Monthly-mean global-mean climate evolution of specific humidity (top) and temperature (bottom) at 300 hPa (left) and 500 hPa (right) over a 5-yr climate simulation interval. Desired climatological accuracies are overplotted as error bars.

Overall the estimated climate measurement performance of the ACE+ baseline constellation, thanks to both its LEO-LEO and GNSS-LEO components together, is expected to allow meeting the climate science objectives laid out in the ACE+ MRD.

4. Summary and Conclusions

This report provided an overview on the scientific retrieval algorithms and the scientific performance of the ACE+ mission. Emphasis was placed on the description of the algorithms and the performance results for the new LEO-LEO technique. The performance assessment was done based on an implementation of the scientific algorithms into an end-to-end performance simulator. The humidity and temperature retrieval results have been assessed relative to the observational requirements laid out in the ACE+ Mission Requirements Document (ACE+ MRD, 2004).

The end-to-end performance simulation system and the scientific algorithms in their current version proved to be adequately mature and suitable for rigorous performance analysis under fairly realistic conditions, including the use of ECMWF high-resolution operational analysis fields, and accounting for cloudy and turbulent conditions. Building on this good status, still a series of further algorithm extensions, improvements, and optimizations should be tackled in

the future, however. Relevant avenues and requirements have been summarized in the LEO-LEO and GNSS-LEO processing description subsections in section 2.

The LEO-LEO performance was found fully compliant with the requirements laid out in the ACE+ MRD, in most cases compliant with the target requirements, including under the adverse conditions of severe atmospheric turbulence below about 3 to 6 km. Compared to GNSS-LEO with its tropospheric temperature–humidity ambiguity, the simultaneous availability of accurate humidity, temperature, and pressure as function of height from LEO-LEO is a particularly intriguing property.

The performance of GNSS-LEO occultations is well established due to the heritage of the observation principle and many studies for previous missions. Starting with the successful GPS/MET "proof-of-concept" mission within 1995 to 1997, the GNSS-LEO technique was extensively evaluated and detailed descriptions of its scientific performance are available from literature. These sources confirm the compliance of GNSS-LEO retrievals with the requirements in the ACE+ MRD.

For both LEO-LEO and GNSS-LEO, the performance results demonstrated the essentially bias-free character of the retrieval products. This key characteristic roots in the self-calibrating nature of the ACE+ data explained in the algorithm descriptions in section 2.

The climate variability and trend measurement performance found for the ACE+ baseline constellation provides evidence, thanks to both the LEO-LEO and GNSS-LEO component together, that the ACE+ climate science goals can be adequately addressed.

The overall conclusion from the scientific performance analyses carried out during Phase A is that ACE+ can fulfill the mission objectives laid out in the ACE+ MRD.

Acknowledgments. The authors thank U. Foelsche, J. Ramsauer, A. Gobiet, A.K. Steiner (all IGAM/UniGraz), M. Gorbunov (IAP Moscow, IGAM/UniGraz), and N. Floury (ESA/ESTEC) for support in preparing various figures of this report and related technical work and for various contributions to the EGOPS5 software. U. Schulzweida (MPI for Meteorology) is thanked for support in the climate constellation analysis and M. Sterenborg (ESA/ESTEC) for Figure 3.3. Valuable comments from P. Silvestrin, T. Wehr (both ESA/ESTEC) and the ACE+ Mission Advisory Group, which improved the report, are gratefully acknowledged. The EGOPS5 software, the core tool of the performance analysis, was developed by an international consortium led by IGAM/UniGraz and involving partner teams at Danish Meteorological Institute, Denmark, Chalmers University of Technology, Sweden, and IEP/University of Bremen, Germany. Also all Colleagues in these partner teams are thanked for their contributions. EGOPS5 is based on strong heritage from EGOPS4, which was developed 1996–2003 by a consortium led by IGAM/UniGraz and involving partner teams at Danish Meteorological Institute and TERMA Elektronik A/S, Denmark, the Met. Office, U.K., and Austrian Aerospace GmbH, Austria, with the major funding provided by ESA. The major funding for producing this report and for the development of EGOPS5 was provided by ESA under ESA/ESTEC Contract No. 16743/02/NL/FF; funds came also from ESA/ESTEC Contract No. 17479/03/NL/FF. Furthermore, co-funding for the work was received from the START research award of G. Kirchengast funded by the Austrian Ministry for Education, Science, and Culture and managed under Program No. Y103-N03 of the Austrian Science Fund.

References

ACE+ MRD, ACE+ Atmosphere and Climate Explorer Mission Requirements Document (for Phase A), *Doc. No. ESD/ACE+/MRD/001/TW-Issue 2 rev. 1*, 51p., ACE+ Mission Advisory Group, ESA/ESTEC, Noordwijk, Netherlands, 2004.

Andersen U., E. Kaas, and P. Alpert, Using analysis increments to estimate atmospheric heating rates following volcanic eruptions, *Geophys. Res. Lett., 28(6)*, 991–994, 2001.

Bengtsson, L., S. Hagemann, and K.I. Hodges, Can climate trends be calculated from re-analysis data?, *J. Geophys. Res.*, accepted, 2004.

ESA, WATS – Water Vapour and Temperature in the Troposphere and Stratosphere, *ESA Publ., ESA, SP-1257(3)*, 2001. [online: www.estec.esa.int/granada_2001 > Assessment reports]

Fjeldbo, G., A. Kliore, and V.R. Eshleman, The neutral atmosphere of Venus as studied with the Mariner V radio occultation experiments, *Astron. J., 76*, 123–140, 1971.

Foelsche, U., and G. Kirchengast, Sensitivity of GNSS occultation profiles to horizontal variability in the troposphere: a simulation study, *Proc. Book, 1st Int'l Workshop on Occultations for Probing Atmosphere and Climate (OPAC-1)*, Sept. 2002, Graz, Austria, Springer Verlag, in press, 2004. [on-line: www.uni-graz.at/igam-arsclisys > Publications]

Gage, K.S., Radar Observations of the Free Atmosphere: Structure and Dynamics, in *Radar in Meteorology (ed. D. Atlas), part II, chap 28*, American Met. Society (AMS) Publ., 534–565, 1990.

Gobiet, A., and G. Kirchengast, Advancement of GNSS radio occultation retrieval in the upper stratosphere, *Proc. Book, 1st Int'l Workshop on Occultations for Probing Atmosphere and Climate (OPAC-1)*, Sept. 2002, Graz, Austria, Springer Verlag, in press, 2004. [on-line: www.uni-graz.at/igam-arsclisys > Publications]

Gorbunov, M. E., Canonical transform method for processing GPS radio occultation data in lower troposphere, *Radio Sci., 37*, 9-1–9-10, doi:10.1029/2000RS002,592, 2002.

Gossard, E.E., Radar Research on the Atmospheric Boundary Layer, in *Radar in Meteorology, part II (ed. D. Atlas), chap 27*, American Met. Society (AMS) Publ., 477–527, 1990.

Gradinarsky, L.P., P. Eriksson, and G. Elgered, ACEPASS Study – Analysis of the impact of clouds-rain-turbulence, *Draft Final ACEPASS WP4.3 Report*, 29p., Chalmers Univ. of Technology, Gothenburg, Sweden, 2003.

GRAS-SAF, *GRAS Meteorology SAF User Requirements*, GRAS-SAF Report, September 2000.

Hajj, G.A., E.R. Kursinski, L.J. Romas, W.I. Bertiger, and S.S. Leroy, A technical description of atmospheric sounding by GPS occultations, *J. Atmos. Sol.-Terr. Phys., 64*, 451–469, 2002.

Healy, S. and J. Eyre, Retrieving Temperature, Water Vapour and Surface Pressure Information from Refractive Index Profiles Derived by Radio Occultation: A Simulation Study, *Quart. J. Roy. Meteorol. Soc., 126*, 1661–1683, 2000.

Hoeg, P., A. Hauchecorne, G Kirchengast, S. Syndergaard, B. Belloul, R. Leitinger, and W. Rothleitner, Derivation of Atmospheric Properties Using a Radio Occultation Technique, *Scient. Rep. 95-4*, DMI, Copenhagen, Denmark, 1995.

Hoeg, P., and G. Kirchengast, ACE+ – Atmosphere and Climate Explorer based on GPS, GALILEO, and LEO-LEO radio occultation (ESA Earth Explorer Opportunity Mission Proposal), *Scient. Rep. 02-07*, DMI, Copenhagen, Denmark, and *Wissenschaftl. Ber. No. 14*, 121p., IGAM, Univ. of Graz, Austria, 2002. [on-line: www.uni-graz.at/igam-arsclisys > Publications]

IPCC, *Climate Change 2001: The Scientific Basis. Contribution of Working Group I to the Third Assessment Report of the Intergovernmental Panel on Climate Change* [Houghton, J.T., Y. Ding, D.J. Griggs, M. Noguer, P.J. van der Linden, X. Dai, K. Maskell, and C.A. Johnson (eds.)]. Cambridge University Press, Cambridge, United Kingdom and New York, NY, USA, 881pp., 2001.

Jensen, A. S., M. S. Lohmann, H.-H. Benzon, and A. S. Nielsen, Full spectrum inversion of radio occultation signals, *Radio Sci., 38*, doi: 10.1029/2002RS002,763, 2003.

Kirchengast, G., J. Hafner, and W. Poetzi, The CIRA86aQ_UoG model: An extension of the CIRA-86 monthly tables including humidity tables and a Fortran95 global moist air climatology model, *Techn. Report for ESA/ESTEC No. 8/1999*, 18p., Inst. Meteorol. Geophys., Univ. of Graz, Austria, 1999. [on-line: www.uni-graz.at/igam-arsclisys > Publications]

Kirchengast, G., J. Fritzer, and J. Ramsauer, End-to-end GNSS Occultation Performance Simulator Version 4 (EGOPS4) Software User Manual (Overview and Reference Manual), *Techn. Report for ESA/ESTEC No. 3/2002*, 472p., IGAM, Univ. of Graz, Austria, 2002. [on-line: www.uni-graz.at/igam-arsclisys > Publications]

Kirchengast, G., S. Schweitzer, J. Ramsauer, J. Fritzer, and M. Schwaerz, Atmospheric Profiles Retrieved from ACE+ LEO-LEO Occultation Data: Statistical Performance Analysis using Geometric Optics Processing, *Tech. Report for ESA/ESTEC No. 1/2004*, IGAM, Univ. of Graz, Austria, 2004. [on-line: www.uni-graz.at/igam-arsclisys > Publications]

Kirchengast, G., and P. Hoeg, The ACE+ Mission: An Atmosphere and Climate Explorer based on GPS, GALILEO, and LEO-LEO Radio Occultation, *Proc. Book, 1st Int'l Workshop on Occultations for Probing Atmosphere and Climate (OPAC-1)*, Sept. 2002, Graz, Austria, Springer Verlag, in press, 2004. [on-line: www.uni-graz.at/igam-arsclisys > Publications]

Kornblueh, L., U. Schulzweida, G. Kirchengast, J. Fritzer, and J. Ramsauer, Final Report of the ACE+ Climate Impact Study – Climate Modeling Part, *Report to ESA/ESTEC*, MPI for Meteorology, Hamburg, Germany, submitted, 2004.

Kuhn, T., TurbScintModel – the EGOPS scintillation model for LEO-LEO occultations, *Draft Report to ESA/ESTEC-Oct.2003*, 22p., IEP, Univ. of Bremen, Germany, 2003.

Kursinski, E.R., G.A. Hajj, J.T. Schofield, R.P. Linfield and K.R. Hardy, Observing Earth's atmosphere with radio occultation measurements using the Global Positioning System, *J. Geophys. Res., 102*, 23,429–23,465, 1997.

Kursinski, E.R., S. Syndergaard, D. Flittner, D. Feng, G. Hajj, B. Herman; D. Ward and T. Yunck, A microwave occultation observing system optimized to characterize atmospheric water, temperature and geopotential via absorption, *J. Atmos. Oceanic Technol., 19(12)*, 1897–1914, 2002.

Kursinski, E.R., D. Feng, D. Flittner, G. Hajj, B. Herman, F. Romberg, S. Syndergaard, D. Ward, and T. Yunck, An active microwave limb sounder for profiling water vapor, ozone, temperature, geopotential, clouds, isotopes and stratospheric winds, *Proc. Book, 1st Int'l Workshop on Occultations for Probing Atmosphere and Climate (OPAC-1)*, Sept. 2002, Graz, Austria, Springer Verlag, in press, 2004.

Lee, L.-C., C. Rocken, and R. Kursinski (Eds), *Applications of Constellation Observing System for Meteorology, Ionosphere & Climate*, Springer Verlag, Hong Kong, 384p., 2001.

Liebe, H.J., G. Hufford, and M. Cotton, Propagation modelling of moist air and suspended water/ice particles at frequencies below 1000 GHz, in *52nd Specialists Meeting of the Electromagnetic Wave Propagation Panel*, p 542, AGARD, 1993.

Marquardt, C., and S. Healy, Validation of GRAS level 1b data, *EUMETSAT Report, WP 2.3*, EUMETSAT, Darmstadt, Germany, 2003.

Melbourne, W.G., E.S. Davis, C.B. Duncan, G.A. Hajj, K.R. Hardy, E.R. Kursinski, T.K. Meehan, L.E. Young, and T.P. Yunck, The application of spaceborne GPS to atmospheric limb sounding and global change monitoring, *JPL Publ. 94-18*, 147 pp., Jet Prop. Lab. Pasadena, Calif., 1994.

Nielsen, A.S., M.S. Lohmann, P. Høeg, H.-B. Benzon, A.S. Jensen, T. Kuhn, C. Melsheimer, S.A. Buehler, P. Eriksson, L. Gradinarsky, C. Jimenez, and G. Elgered, Characterization of ACE+ LEO-LEO Radio Occultation Measurements, *ESTEC contract no. 16743/02/NL/FF*, 2003. [online: ftp://ftp.estec.esa.int/pub/eopp/pub/ACEplus]

Rieder, M.J., and G. Kirchengast, Error analysis and characterization of atmospheric profiles retrieved from GNSS occultation data, *J. Geophys. Res., 106*, 31,755–31,770, 2001.

Rocken, C., R. Anthes, M. Exner, D. Hunt, S. Sokolovskiy, R. Ware, M. Gorbunov, W. Schreiner, D. Feng, B. Herman, Y.H. Kuo, and X. Zou, Analysis and validation of GPS/MET data in the neutral atmosphere, *J. Geophys. Res., 102*, 29,849–29,866, 1997.

Rodgers, C., *Inverse methods for atmospheric sounding: theory and practice*, 256 pp., Word Sci., River Edge, N.J., 2000.

Roeckner, E., L. Bengtsson, J. Feichter, J. Lelieveld, and H. Rodhe, Transient climate change simulations with a coupled atmosphere-ocean GCM including the tropospheric sulfur cycle, *J. Climate, 12*, 3004–3032, 1999.

Smith, E.K. and S. Weintraub, The constants in the equation of atmospheric refractive index at radio frequencies, *Proc. of the I.R.E., 41(8)*, 1035–1037, 1953.

Sokolovskiy, S. V., Tracking tropospheric radio occultation signals from low earth orbit, *Radio Sci., 36* , 483–498, 2001.

Steiner, A.K., G. Kirchengast, and H.P. Ladreiter, Inversion error analysis and validation of GPS/MET occultation data, Ann. Geophys., 17, 122–138, 1999.

Steiner, A.K., G. Kirchengast, U. Foelsche, L. Kornblueh, E. Manzini, and L. Bengtsson, GNSS occultation sounding for climate monitoring, *Phys. Chem. Earth (A), 26*, 113–124, 2001.

Steiner, A.K., and G. Kirchengast, Ensemble-based analysis of errors in atmospheric profiles retrieved from GNSS occultation data, *Proc. Book, 1st Int'l Workshop on Occultations for*

Probing Atmosphere and Climate (OPAC-1), Sept. 2002, Graz, Austria, Springer Verlag, in press, 2004. [on-line: www.uni-graz.at/igam-arsclisys > Publications]

Syndergaard, S., Retrieval analysis and methodologies in atmospheric limb sounding using the GNSS radio occultation technique, *DMI Sci. Rep. 99-6*, 131 pp., Danish Meteorological Inst., Copenhagen, Denmark, 1999.

Syndergaard, S, D. Flittner, R. Kursinski, D. Feng, B. Herman and D. Ward, Simulating the influence of horizontal gradients on retrieved profiles from ATOMS occultation measurements: a promising approach for data assimilation, *Proc. Book, 1st Int'l Workshop on Occultations for Probing Atmosphere and Climate (OPAC-1)*, Sept. 2002, Graz, Austria, Springer Verlag, in press, 2004.

Zou, X., F. Vandenberghe, B. Wang, M. Gorbunov, Y.-H. Kuo, S. Sokolovsky, J. Chang, J. Sela, C. Lee and R. Anthes, A raytracing operator and its adjoint for the use of GPS/MET refraction angle measurements, *J. Geophys. Res.*, *104*, 22,301–22,318, 1999.

Ω end of document Ω